

**MAGNESIUM ALLOYS FOR USE AS AN INTRALUMINAL TRACHEAL STENT**

by

**Sarah Anne Luffy**

Bachelor of Biomedical Engineering, The Catholic University of America, 2009

Submitted to the Graduate Faculty of  
Swanson School of Engineering in partial fulfillment  
of the requirements for the degree of  
Master of Science

University of Pittsburgh

2013

UNIVERSITY OF PITTSBURGH  
SWANSON SCHOOL OF ENGINEERING

This thesis was presented

by

Sarah Anne Luffy

It was defended on

March 12, 2013

and approved by

Prashant Kumta, PhD

Edward R. Weidlein Chair Professor, Departments of Bioengineering, Chemical and  
Petroleum Engineering, Mechanical Engineering and Materials Science

Jenora Waterman, PhD

Assistant Professor, Department of Animal Sciences, NCA&T

Peter Wearden MD, PhD

Assistant Professor, Department of Cardiothoracic Surgery

Thesis Advisor: Thomas Gilbert, PhD

Adjunct Professor, Department of Bioengineering

Copyright © by Sarah Anne Luffy

2013

# **MAGNESIUM ALLOYS FOR USE AS AN INTRALUMINAL TRACHEAL STENT**

Sarah Anne Luffy, M.S.

University of Pittsburgh, 2013

Tracheal stenting is used for successful management of adult airway obstructions, including tracheal stenosis, a narrowing of the tracheal lumen due to trauma or prolonged intubation. The permanent nature of non-degradable tracheal stents makes them a treatment option of last resort for pediatric patients. Complications associated with stent removal and restenosis could be avoided with degradable tracheal stent placement. Magnesium alloys are demonstrating promise as degradable materials in orthopedic and cardiovascular applications, however the performance of magnesium alloys in the trachea remains unknown. This research explores three commercially available magnesium alloys for evaluation as degradable tracheal stents. The degradation behavior of these alloys was first evaluated *in vivo* as an intraluminal stent in a rat tracheal bypass model. Even after 6 months the stents persisted and degradation was assessed using microCT imaging. Significant differences in percent of total volume lost were found between alloys over time. Magnesium alloys were also evaluated in a bioreactor to simulate the airway environment and corrosion *in vitro*. Using ICP, the presence of magnesium from each alloy was measured in a simulated airway media and in a control media over 7 days. Significant differences in corrosion were observed between the simulated and control conditions for *in vitro* assessment of each alloy. Additionally, *in vitro* corrosion of magnesium alloys did not appear significantly different from the percent of total volume lost *in vivo* at the 1-week time point. This study demonstrates an approach to evaluating magnesium alloys as intraluminal tracheal stents. Further development of the alloys and stent design are required for a clinically translatable model.

## TABLE OF CONTENTS

<b>NOMENCLATURE.....</b>	<b>X</b>
<b>PREFACE.....</b>	<b>XI</b>
<b>1.0 INTRODUCTION.....</b>	<b>1</b>
<b>1.1 ANATOMY OF THE TRACHEA .....</b>	<b>1</b>
<b>1.1.1 Management of Tracheal Stenosis .....</b>	<b>3</b>
<b>1.1.2 Need for a Degradable Tracheal Stent .....</b>	<b>4</b>
<b>1.1.3 Historical Applications of Magnesium .....</b>	<b>7</b>
<b>1.1.4 Magnesium Alloys for Tracheal Stents.....</b>	<b>9</b>
<b>1.2 RESEARCH OBJECTIVES.....</b>	<b>10</b>
<b>1.2.1 Aims and Hypotheses .....</b>	<b>10</b>
<b>1.2.1.1 Specific Aim 1: To determine the in vivo degradation patterns of magnesium alloys in a tracheal location.....</b>	<b>10</b>
<b>1.2.1.2 Specific Aim 2: To determine the in vitro degradation of magnesium alloys.....</b>	<b>11</b>
<b>2.0 EVALUATION OF MAGNESIUM ALLOYS IN VIVO.....</b>	<b>12</b>
<b>2.1 IN VIVO STUDY DESIGN AND METHODS .....</b>	<b>12</b>
<b>2.1.1 In vivo study design .....</b>	<b>12</b>
<b>2.1.1 Methods .....</b>	<b>13</b>

2.1.1.1	Materials Preparation.....	13
2.1.1.2	Surgical Procedure.....	14
2.1.1.3	Post-Operative Care .....	15
2.1.1.4	Assessment of Corrosion In Vivo.....	15
2.1.1.5	Histological Evaluation.....	16
2.1.1.6	Statistical Analysis .....	17
2.2	RESULTS .....	17
2.2.1	Pure Mg .....	17
2.2.1.1	Stent Volume Lost.....	17
2.2.1.2	Histological Evaluation.....	19
2.2.2	AZ31.....	23
2.2.2.1	Stent Volume Lost.....	23
2.2.2.2	Histological Evaluation.....	24
2.2.3	MgY.....	28
2.2.3.1	Stent Volume Lost.....	28
2.2.3.2	Histological Evaluation.....	29
2.3	SUMMARY OF IN VIVO RESULTS .....	33
3.0	EVALUATION OF MAGNESIUM ALLOYS IN VITRO .....	35
3.1	IN VITRO STUDY DESIGN AND METHODS.....	35
3.1.1	Assessment of Corrosion in vitro .....	36
3.1.1.1	ICP Analysis .....	36
3.1.1.2	MicroCT Analysis .....	37
3.1.1.3	Statistical Analysis .....	37

<b>3.2</b>	<b>RESULTS .....</b>	<b>38</b>
<b>3.2.1</b>	<b>ICP Results .....</b>	<b>38</b>
<b>3.2.1.1</b>	<b>Pure Mg.....</b>	<b>38</b>
<b>3.2.1.2</b>	<b>AZ31 .....</b>	<b>39</b>
<b>3.2.1.3</b>	<b>MgY .....</b>	<b>41</b>
<b>3.2.2</b>	<b>MicroCT Analyses .....</b>	<b>42</b>
<b>3.2.2.1</b>	<b>Pure Mg.....</b>	<b>43</b>
<b>3.2.2.2</b>	<b>AZ31 .....</b>	<b>44</b>
<b>3.2.2.3</b>	<b>MgY .....</b>	<b>45</b>
<b>3.2.3</b>	<b>Statistical Analysis.....</b>	<b>45</b>
<b>3.3</b>	<b>SUMMARY OF IN VITRO RESULTS.....</b>	<b>46</b>
<b>4.0</b>	<b>DISCUSSION .....</b>	<b>47</b>
<b>5.0</b>	<b>CONCLUSIONS .....</b>	<b>51</b>
	<b>BIBLIOGRAPHY .....</b>	<b>52</b>

## LIST OF FIGURES

- Figure 1. Anatomy of the human trachea from the larynx to the bronchi, with a cross section showing the inner to outer layers of the trachea. .... 2
- Figure 2. AZ31 tracheal stent is represented in this image, but all stents were machined with outer diameter of 2.25mm, inner diameter of 1.25mm and length of 5mm..... 13
- Figure 3. Surgical placement of an intraluminal tracheal stent in a Lewis rat trachea. A tracheal bypass model was used to evaluate the stent in vivo. .... 15
- Figure 4. MicroCT image with 3-dimensional reconstruction using Mimics software..... 16
- Figure 5. Percent of total volume lost during in vivo testing for each alloy at 1, 8, 16 and 24 weeks. Significant differences among alloys and between time points are indicated by the v, \*, and #..... 18
- Figure 6. Representative images of 3-dimentional microCT volumes for Pure Mg stents prior to implantation and at the 1, 8, 16, and 24 week time points..... 19
- Figure 7. A) Representative histology (H&E) from Pure Mg stents in vivo at 1 week. Cross sectional image of tracheal bypass taken to show differences in native epithelium (left) and the stented airway epithelium (right). Arrow indicates the beginning of stent incorporation. B) Boxed area of stented airway epithelium from (A) shown with higher magnification. No cilia present, but strong mononuclear presence..... 20
- Figure 8. Representative images of 3-dimentional microCT volumes for AZ31 stents prior to implantation and at the 1, 8, 16, and 24 week time points..... 24



Figure 9. A) Representative histology (H&E) from AZ31 stents in vivo at 1 week. Cross sectional image of stented trachea showing mononuclear cell population. B) Boxed area from (A) shown with higher magnification to display disruption of epithelium, most likely due to surgical placement of the stent. .... 25

Figure 10. Representative images of 3-dimmesional microCT volumes for MgY stents prior to implantation and at the 1, 8, 16, and 24 week time points..... 29

Figure 11. A) Representative histology (H&E) from MgY stents after 1 week in vivo. Hypercellularity in the native tracheal epithelium with the presence of possible giant cells. B) Boxed area from (A) shown with higher magnification. Epithelium is disrupted and arrow indicates possible giant cell. .... 30

Figure 12. ICP results for each alloy showing magnesium concentration measured in SAF and in saline. Results represent averages of n=3 samples for each alloy at each time point. No significant differences were found among alloys under saline conditions, while results from Pure Mg were significantly different (❖) from AZ31 and MgY under SAF conditions..... 38

Figure 13. ICP results for Pure Mg tracheal stents, displaying average magnesium concentrations (n=3) at 1, 3, 5, and 7 days in vitro for both SAF and saline conditions. .... 39

Figure 14. ICP results for AZ31 tracheal stents, displaying average magnesium concentrations (n=3) at 1, 3, 5, and 7 days in vitro for both SAF and saline conditions. .... 41

Figure 15. ICP results for MgY tracheal stents, displaying average magnesium concentrations (n=3) at 1, 3, 5, and 7 days in vitro for both SAF and saline conditions. .... 42

Figure 16. Bar graph summarizing the comparison of corrosion after 1 week in vivo to 1 week in vitro under both SAF and saline conditions. The (#) indicates significant differences were observed between all alloys under the saline in vitro control conditions, while the (\*) indicates only Pure Mg experienced significantly different results under SAF in vitro conditions. .... 43

Figure 17. Representative 3-dimensional microCT images of Pure Mg, AZ31, and MgY stents after 1 week of in vitro testing in SAF media and saline control conditions..... 44

## **NOMENCLATURE**

ANOVA – analysis of variance

ICP – inductively coupled plasma

H&E – hematoxylin and eosin

PAS – periodic acid shift

MgY – magnesium yttrium

AZ31 – aluminum zinc magnesium alloy with 3% aluminum and 1% zinc

Mg - magnesium.

SAF – simulated airway fluid

SEMS – self-expanding metallic stent

## **PREFACE**

Thank you to the members of my committee for your guidance, encouragement, and support. A special thank you to my thesis adviser and graduate mentor, Dr. Thomas Gilbert. This work was part of the National Science Foundation Engineering Research Center for Revolutionizing Metallic Biomaterials (NSF ERC-RMB). The magnesium ingots containing yttrium were obtained from Helmholtz-Zentrum Geesthacht, Institute of Materials Research, Geesthacht, Germany through a gracious gift from Dr. Norbert Hort and Dr. Frank Witte. The machining expertise for the manufacturing of the tracheal stents was provided by Mr. Andrew Holmes at the University of Pittsburgh Swanson Center for Product Innovation (SCPI).

## 1.0 INTRODUCTION

### 1.1 ANATOMY OF THE TRACHEA

Characterized as a hollow, single lumen tube, the trachea allows for air passage from the larynx to the bronchi. C-shaped cartilage rings provide the rigid structure necessary to support the trachea and prevent collapse during the breathing process. The posterior wall of the trachea contains smooth muscle, which offers flexibility in addition to preventing over distension of the airway during expiration. Mechanical ventilation is the primary function of the trachea, but the intraluminal mucosal lining of the trachea provides clearance pathways for bronchial secretions. A heterogeneous cell layer including pseudostratified columnar epithelial cells, including ciliated cells, secretory and goblet cells, and basal cells create the inner most layer of the tracheal wall. The basement membrane is subjacent to the epithelial cell layer, which lies against the connective tissue and smooth muscle cells followed by the cartilage rings<sup>1</sup>, **(Figure 1)**.

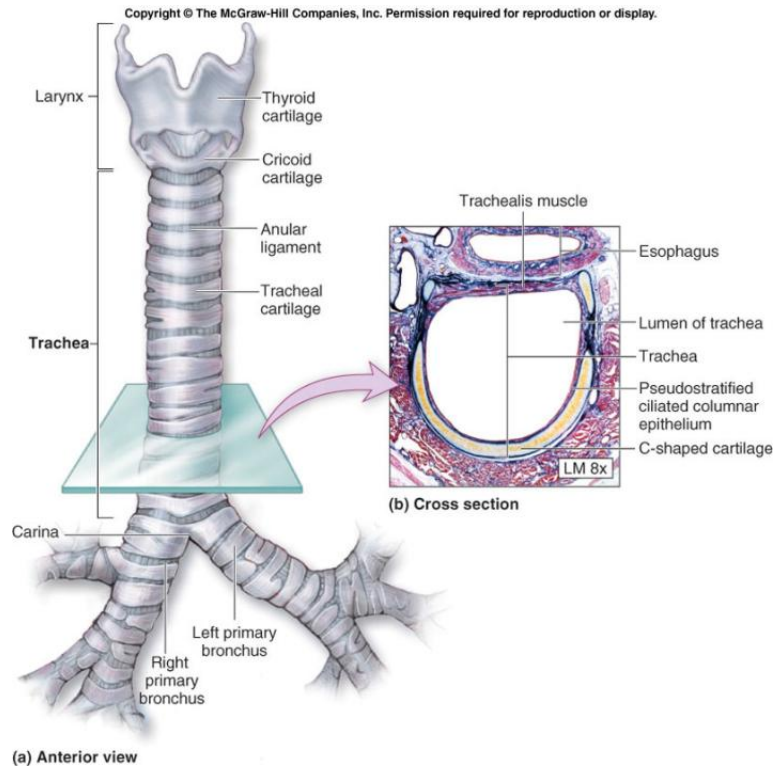


**Figure 1. Anatomy of the human trachea from the larynx to the bronchi, with a cross section showing the inner to outer layers of the trachea.**

For diagnostic purposes, airway obstructions are classified based on the location of the disease and referenced as upper airway obstructions and lower airway obstructions. The trachea is considered part of the upper airway, which is described as the region between the nose and the trachea. Because there is no official clinical classification of a “middle airway,” the trachea is considered closer to the upper airway than the lungs<sup>2</sup>.

Tracheal obstructions are presented in both congenital and acquired instances. Congenital anatomical anomalies can result in airway obstruction, as in cases of pulmonary artery sling, where the left pulmonary artery placement is between the trachea and esophagus. The left pulmonary artery grows towards the left lung and causes compression on the lower trachea, often resulting in the occurrence of complete tracheal rings. This weakening of the tracheal cartilage

leading to collapse of the airway is described as tracheomalacia<sup>3,4</sup>. Tracheal obstructions are rare, but acquired tracheal obstructions are more common in children than congenital cases and are often the result of long-term intubation<sup>5,6</sup>. Severe cases of tracheal obstruction resulting from acquired stenosis, often require multiple surgical and endoscopic procedures to achieve long-term goals of a desirable outcome<sup>7</sup>.

### **1.1.1 Management of Tracheal Stenosis**

Injury to the lumen of the trachea typically leads to the formation of scar tissue that can cause tracheal obstruction through a narrowing of the tracheal lumen. The condition is called tracheal stenosis<sup>8</sup>. Tracheal stenosis can be the result of a congenital disorder, but more often it is acquired from prolonged intubation, trauma, a tumor, or infection<sup>9</sup>. Although tracheal obstructions are rare among the pediatric patient population, pediatric tracheal stenosis is associated with severe morbidity and mortality, and the management of stenosis consistently challenges clinicians<sup>10,11</sup>.

Endoscopic management of tracheal stenosis by balloon dilation is used as a method of treatment when attempting to avoid open surgical procedures in both children and adults<sup>12</sup>. However, the effects of balloon dilation on the stenotic trachea are poorly understood, and repeated treatments are often necessary. Surgical management of tracheal stenosis in adults is commonly practiced by resection of the compromised trachea with primary reconstruction by end-to-end anastomosis. Reconstruction is a primary treatment option for pediatric patients, however because of the small size of the pediatric airway, children do not experience the same success with resection and end-to-end anastomosis that adults can achieve<sup>13</sup>. Ischemia and

anastomotic tension resulting from reconstruction can cause restenosis. Slide tracheoplasty has become the treatment of choice when surgery is necessary. While alternative temporary or definitive methods are being developed for those who are not surgical candidates, surgical reconstruction is still considered the ideal approach for management of tracheal stenosis<sup>14</sup>. In order to avoid a reoccurrence of tracheal stenosis following surgical repair, tracheal stents have been used with reasonable success. Minimally invasive deployment options for intraluminal balloon expandable stents have become an attractive option for treatment of tracheal stenosis. Complications associated with tracheal stenting include encapsulation and incorporation into the mucosal tissue, migration, perforation, and compromised mucociliary clearance of the airway<sup>9,15</sup>.

### **1.1.2 Need for a Degradable Tracheal Stent**

Tracheal stents are classified as equivalent to tracheal prostheses under FDA guidelines for medical device approval. Intentions for use of a tracheal stent must include the maintenance of airway patency. Stenosis from prolonged intubation, tracheal burn or trauma, tracheobronchomalacia, and external compression of the trachea are the most common conditions responsive to stent placement<sup>16</sup>. Stents are more broadly used in the context of vascular medicine. A stent is defined by the National Institutes of Health (NIH) in the context of a coronary stent as a mesh tube used to support weak arteries<sup>41</sup>. Coronary stents vary in size, geometry, function, and deployment method. Following angioplasty, a procedure using a balloon to dilate the blood vessels compromised by disease or plaque, stents are placed in about 60 percent of cases to support the vessel and prevent restenosis<sup>17</sup>. Restenosis is a reduction of the vessel lumen by greater than 50 percent at the area of previous treatment<sup>18,19</sup>. In-stent restenosis (ISR) still persists in about 25 percent of stents placed following angioplasty<sup>17</sup>. Depending on the

diagnosis, a variety of stents may be used for treatment of a compromised vessel. Percutaneous intervention allows for placement of self-expanding, balloon expandable, and drug-eluting stents ranging in material composition.

Tracheal stents currently available vary in material composition and physical geometry, as well as application purpose. Stent selection typically depends on whether the patient has a benign or malignant disease, the need for the stent is temporary or permanent, the physician's experience with stent insertion, and finally, the cost of the procedure<sup>20</sup>. For a pediatric case involving the onset of long segment stenosis following tracheostomy, surgical resection was used to remove the stenosis and release the trachea, followed by reconstruction and placement of a silicone Dumon stent<sup>21</sup>. In 2007, one retrospective study focused on Dumon stent use in 35 patients. The Japanese study found the Dumon stent the most effective tracheal stent for treatment of both tracheal stenosis and airway fistulas, based on cost and safety<sup>20</sup>. Although the stent is made from radiopaque silicone and the design features include external struts to prevent migration, it is a permanent silicone implant. Even with surface treatments designed to maximize mucociliary clearance and minimize the risk of obstruction, the described study still included multiple patients who experienced migration, obstruction, and restenosis<sup>20</sup>.

Self-expanding metallic stents, or SEMS, offer properties consistent with the ideal design requirements for a tracheal stent – easy insertion, biocompatible, non-obstructive, does not inhibit mucociliary clearance, and adapts to the varying dimensions of the airway during respiration and coughing<sup>22</sup>. The consistent problem with metallic stents, as with all stents, is their permanent nature and difficult removal despite these positive features. In addition, the very nature of SEMS can be problematic over time as the stent continually applies an outward



pressure on the trachea that can lead to perforation. Problems and complications associated with stent removal make pediatric tracheal stenting a treatment option of last resort<sup>14,15</sup>. When surgical intervention is limited, SEMS have shown reasonable success in the airway, but SEMS use should be avoided in the treatment of benign airway obstructions, as in the case of laryngotracheal airway obstruction<sup>23</sup>. In fact, stent related complications are often more difficult to treat than the original indication for initial stent placement<sup>24</sup>. In the pediatric patient population, even the most widely accepted tracheal stents succumb to the complications of granulation tissue, obstruction, and fracture after just 2 weeks<sup>11</sup>.

Tracheal stenting is used for management of adult airway obstructions, but because non-degradable stents are considered permanent implants after encapsulation, they are considered a treatment option of last resort for children. The pediatric population requires growth potential over time, and the permanent nature of a non-degradable stent increases the likelihood of complications associated with stent removal and restenosis. In fact, the pediatric population experiences an estimated stent related mortality of 12.9%<sup>15</sup>. A degradable stent would allow for growth potential while supporting an open tracheal lumen, making it an ideal treatment option for pediatric tracheal stenosis. Biodegradable stents have been developed for use in esophageal, urethral, and intestinal stenosis, while biodegradable stents for treatment of tracheal stenosis has been used experimentally<sup>25</sup>. One study presents the use of a polydioxanone tracheobronchial degradable stent as an alternative to metallic or silicone stents for the treatment of stenosis<sup>25</sup>.

Permanent stent alternatives are also being investigated for cardiovascular stent design using degradable metallic materials. As with the trachea, the need for a coronary stent is temporary and a degradable material could decrease the risk of complications associated with permanent implants. Coronary stents made from stainless steel, nitinol, and cobalt-chromium

alloys have shown success, but more widespread use is limited by their permanent nature, thrombogenicity, inflammatory response, potential to cause perforation, and inability to provide for growth potential<sup>17</sup>. Iron based biodegradable stents are believed to be a suitable material for coronary stents because of the ability of iron to bind oxygen molecules, and especially as a larger size stent because of its robust nature and strong mechanical properties throughout the degradation period<sup>17</sup>. Biodegradable stents have demonstrated feasibility in early studies<sup>26,27</sup>, and while magnesium alloys have historically been used in orthopedic fixation devices<sup>28,29</sup>, they are showing promise in cardiovascular applications. These applications include a multi-center clinical trial of magnesium stents<sup>30-32</sup>. The multi-center human clinical trial described the use of a balloon-expandable magnesium based coronary stent for treatment of coronary artery lesions.

### **1.1.3 Historical Applications of Magnesium**

Magnesium is a common biometal, naturally occurring in the human body and essential for life. Critical in many enzymatic reactions, magnesium and calcium also work together to regulate neuromuscular transmission<sup>33</sup>. Additionally, magnesium promotes relaxation of the airway by inhibiting the influx of calcium ions and blocking the voltage-dependent calcium channels<sup>33</sup>. The presence of magnesium and magnesium sulfates in the airway has led to positive outcomes in the treatment of pediatric asthma by increasing lung function and reducing hospitalization<sup>34</sup>.

Sir Humphrey Davy discovered elemental magnesium in 1808, and magnesium has been investigated as a degradable biomaterial for over 100 years<sup>29</sup>. Magnesium wires were first implanted in humans as ligatures to control the bleeding of human vessels, where it was discovered that corrosion of Mg was slower in vivo and that the time for degradation corresponded directly to the size of the Mg wire<sup>17,29</sup>. Pure Mg wire was too brittle to serve as a

suture material, which prompted the development of magnesium alloys. Absorbable magnesium staples and clips were used to ensure hemostasis in many applications such as intestinal anastomosis and deep wound closure<sup>29,35</sup>. When used as a screw for bone fixation, the first human clinical study reported completed resorption of magnesium after 1 year with physiological bone healing and benign gas evolution that disappeared a few weeks after implantation, according to x-ray<sup>29</sup>. The combination of these early clinical studies found magnesium non-toxic and a non-irritant, but emphasized the importance of separating magnesium implants from other metals due to the risk of electrolytic corrosion<sup>29</sup>. The corrosion product of magnesium oxide was believed early on to promote bone and callus formation. Investigators believed that inserting magnesium into inflammatory tissue of pseudarthrosis cases allowed for the neutralization of the acidic environment, which lead to the formation of callus bone and healing<sup>17,29,36</sup>. Inflammation following magnesium implantation appears consistent throughout historical studies, leading to fibrous encapsulation of the corroding magnesium, especially in bone tissue<sup>29</sup>. Early use of magnesium in vessels and subcutaneous tissue resulted in vascularized granulation tissue surrounding the magnesium implant, as well as localized foreign body giant cells and leukocytes. Interestingly, no infections were reported during the early investigational uses of magnesium implants<sup>29</sup>. Important insights into magnesium corrosion were observed during these initial studies. Total absorption of magnesium, for example, was found to depend more on the exposed surface of the metal than on the total weight of the metal, as indicated by comparing magnesium wires and sheets to thicker pieces with the same surface area<sup>29,36</sup>. Although consistencies in corrosion rate of magnesium among tissue type and species remain unpredictable, the corrosion rate does appear to depend on the size of the magnesium implant and the tissue type in which it was imbedded<sup>29,35</sup>. Even early investigators postulated the

corrosion of magnesium to be dependent on an oxidation process that was directly related to oxygen content in the blood, as well as the water content of the surrounding tissue and the local hydrogen carbonic acid content. Regardless of the magnesium metals used throughout the early history of magnesium implants, a non-toxic, non-irritant, and non-carcinogenic result of magnesium oxides and magnesium phosphates were found<sup>17,29</sup>. Advancements in science and medicine throughout recent history are only now beginning to produce magnesium implants for use in clinical trials.

#### **1.1.4 Magnesium Alloys for Tracheal Stents**

The history of magnesium showed its potential for use as a degradable biomaterial. Magnesium is also known to have low thrombogenicity and strong biocompatibility due to its naturally occurring presence in the human body<sup>17</sup>. Because magnesium can experience fast degradation and loss of mechanical properties, it is alloyed with other elements, like aluminum, to decrease the rate of degradation<sup>37</sup>. Magnesium alloys degrade in aqueous environments and are resorbed by the body through oxidation making them attractive materials for the development of a degradable tracheal stent. Yttrium has been used as an alloying element in magnesium cardiovascular stents with <5% yttrium and has showed results of endothelialization, minimal inflammation, and stent degradation within approximately 90 days<sup>38</sup>. Alloys containing aluminum and zinc have been shown to increase resistance to corrosion in vitro<sup>39</sup>.

The performance of magnesium alloys in the trachea remains unknown. The response of the tracheal tissue to the presence of magnesium cannot be predicted without adequate models. Furthermore, standard in vitro corrosion assays inaccurately predict in vivo behavior of magnesium alloys<sup>40,21</sup>. The objective of this research is to evaluate the degradation behavior of

three commercially available magnesium alloys: Mg3Y, AZ31, and 99.9% Pure Mg. First, a specially developed rat tracheal bypass model was used to allow for evaluation of the stent materials in the airway without risk of death due to airway obstruction. In vitro analysis was then conducted using a bioreactor with simulated airway fluid containing mucins to simulate the airway environment. The in vitro results were then compared to the in vivo degradation kinetics to determine a correlation between degradation of magnesium alloys in the airway. MgY was evaluated in a previous study as an extraluminal tracheal stent for the treatment of tracheomalacia (appendix). This study showed that the body could tolerate the presence of an extraluminal stent with a mild host response, without negatively impacting the native cartilage after 8 weeks.

## **1.2 RESEARCH OBJECTIVES**

### **1.2.1 Aims and Hypotheses**

#### **1.2.1.1 Specific Aim 1: To determine the in vivo degradation patterns of magnesium alloys in a tracheal location.**

Hypothesis: Each of the alloys are expected to have different corrosion behaviors, with the AZ31 and MgY stents experiencing slower degradation than the Pure Mg at both early and late time points. It is hypothesized that histological evaluation will reveal minimal host response to the stent with the trachea maintaining patency and a healthy airway epithelium.

**1.2.1.2 Specific Aim 2: To determine the in vitro degradation of magnesium alloys.**

Hypothesis: The amount of magnesium present in the media after 1 week is expected to correspond to the total volume loss of the stent in vivo at the 1-week time point.

## **2.0 EVALUATION OF MAGNESIUM ALLOYS IN VIVO**

### **2.1 IN VIVO STUDY DESIGN AND METHODS**

#### **2.1.1 In vivo study design**

All animal experiments were reviewed and approved by the University of Pittsburgh Institutional Animal Care and Use Committee and were performed in compliance with the Guide for the Care and Use of Laboratory Animals (NIH Publication #85-23 Rev. 1985, *Lab Animal* 23(8):28-29,1994). Female Lewis rats, ranging in weight from 150 to 350g (Charles River), were used in this study for the evaluation of three different magnesium alloys as degradable intraluminal tracheal stents. A machinable, non-balloon expandable stent geometry was designed to evaluate the degradable alloys *in vivo* through the design of a tracheal bypass model. The alloys were evaluated at 1, 8, 16, and 24-week time points. Upon explant the stent-tissue complex was imaged using microCT and processed to analyze volume loss and stent geometry over time. Explants were prepared for histological analysis using paraffin processing.

## 2.1.1 Methods

### 2.1.1.1 Materials Preparation

Commercially available 99.9% pure magnesium was obtained from Goodfellow (Coraopolis, PA, USA) and used as the first material for evaluation as an intraluminal tracheal stent. Magnesium containing 3% aluminum and 1% zinc, also obtained from Goodfellow, was considered as a second material for stent evaluation in this study. The third material for an intraluminal tracheal stent was magnesium containing 3 wt% Y (W3) obtained from Helmholtz Zentrum Geesthacht Institute of Materials Research, Geesthacht, Germany, provided as a gift from Dr. Norbert Hort and Dr. Frank Witte. All three materials were T4 heat treated at 525 °C under a protective environment of Ar + 0.1% SF<sub>6</sub> for 8 h to homogenize intermetallics and alloying elements in the alloy matrix. The magnesium alloys were machined into stents at the University of Pittsburgh Swanson School for Product Innovation (SCPI), with an outer diameter of 2.25mm, inner diameter of 1.25mm and length of 5mm, **Figure 2**.



**Figure 2.** AZ31 tracheal stent is represented in this image, but all stents were machined with outer diameter of 2.25mm, inner diameter of 1.25mm and length of 5mm.



To remove stresses imparted by the machining process, the stents were then subjected to a second heat treatment at 205°C for 1.5h in ultra high purity argon (UHP-Ar). All stents were sonicated in isopropanol for 5 minutes and dried in air (3x), and then terminally sterilized with 2MRad  $\gamma$ -irradiation.

### **2.1.1.2 Surgical Procedure**

Donor female Lewis rats were anesthetized by intraperitoneal injection of ketamine (80 mg/kg) xylazine (8 mg/kg) to maintain the surgical plane of anesthesia, and were euthanized via exsanguination. The tracheas were harvested to provide a bypass surgical model for stent evaluation, **Figure 3**. Recipient animals were anesthetized in a similar way. Aseptic technique was used to expose the proximal cervical trachea through a midline neck incision. Small proximal and distal defects separated by 5 cartilage rings were created in the recipient trachea. The stent was placed intraluminally in the donor trachea, which was anastomosed to the distal and then proximal defects using 7-0 prolene suture (Ethicon, Somerville, NJ). The bypass model allowed for airway communication and evaluation of the non-optimized stent geometries *in vivo* without compromising respiration. The skin incision was closed using an interrupted suturing technique with 5-0 PDS suture (Ethicon, Somerville, NJ). Proper anastomosis was determined by visual inspection and by the absence of any sub-cutaneous air upon closure.

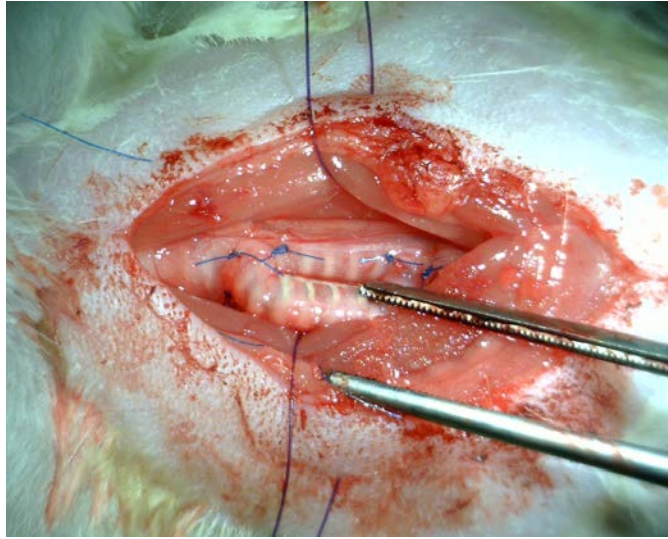


**Figure 3. Surgical placement of an intraluminal tracheal stent in a Lewis rat trachea. A tracheal bypass model was used to evaluate the stent in vivo.**

### **2.1.1.3 Post-Operative Care**

All animals were recovered from anesthesia and monitored until alert and active. In the immediate post-operative period, buprenorphine hydrochloride (0.05 mg/kg, Butler Schein) was administered every 12 hours for 5 days for pain management.

### **2.1.1.4 Assessment of Corrosion In Vivo**

Using micro computed tomography ( $\mu$ CT), Inveon (Siemens, Munich, Germany), the magnesium stents were imaged prior to implantation, **Figure 4**. Upon harvest of the trachea-stent complex, the tissue was fixed in formalin and subjected to the same  $\mu$ CT imaging. The 2-dimensional Dicom files were processed using Mimics software (Materialise, Mimics 12.01, Belgium). Three-dimensional volumes of the stents were generated for the data prior to implantation and at 1, 8, 16, and 24 week explants. The difference in volume ( $\text{mm}^3$ ) was calculated and an overall

percent of total volume lost over time quantified. The total volume loss served as an indication of the corrosion behavior of the stent in vivo. Statistical analysis was performed to determine significant differences between original stent volume and stent volume at each end point for each alloy in this study.

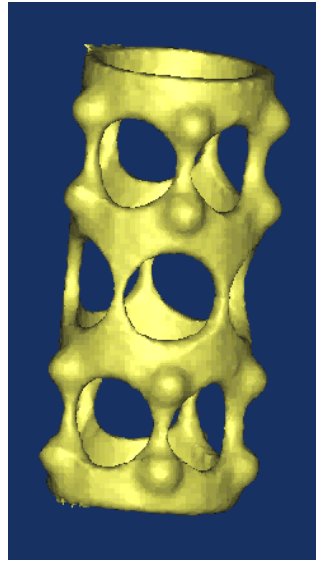


**Figure 4. MicroCT image with 3-dimensional reconstruction using Mimics software**

#### **2.1.1.5 Histological Evaluation**

The stented trachea bypass complex was harvested and fixed in 10% neutral buffered formalin (NBF), dehydrated, and embedded in paraffin for histological analysis. Cross-sectional tissue specimens were cut along the longitudinal axis of the trachea-stent bypass in 5-micron sections. Following deparaffinization and rehydration, sections of the trachea-stent complex were stained with Hematoxylin and Eosin (H&E), Masson's Trichrome, Alcian Blue, and Periodic acid-Schiff (PAS).

### 2.1.1.6 Statistical Analysis

All statistical analyses were performed using the SPSS package (version 20.0; IBM SPSS, Inc, Chicago, Ill). Statistical significance was set at  $p < 0.05$ .

To compare the differences of in vivo corrosion within and between the alloy groups over time, a two-way independent ANOVA with Tukey's Post Hoc analysis was used to analyze the percent of total stent volume lost in each animal. Percent of total stent volume lost over time is reported as mean  $\pm$  standard deviation.

## 2.2 RESULTS

### 2.2.1 Pure Mg

#### 2.2.1.1 Stent Volume Lost

Pure Mg showed a volume loss at 1-week of 6.3%  $\pm$  1.6%. At 8 weeks, the volume loss was 34.1%  $\pm$  15.7%, which was not a significant increase in mass loss compared to 1-week. The volume loss continued to increase through 16 weeks to 65.9%  $\pm$  7.9%, a significant increase from the 1 and 8-week time points. Pure Mg showed the greatest volume loss of the three alloys tested at 16 weeks, (**Figure 5**). After 24-weeks, the volume loss of 64.2%  $\pm$  16.8% was similar to the 16 week results. Representative structures of the Pure Mg stent at each time point are illustrated in **Figure 6**. The structure of the stent was preserved after 1-week, but after 8-weeks

stent fracture and significant volume loss had occurred. By 16 and 24 weeks, the stent structure was completely compromised and only fragments of material remained.

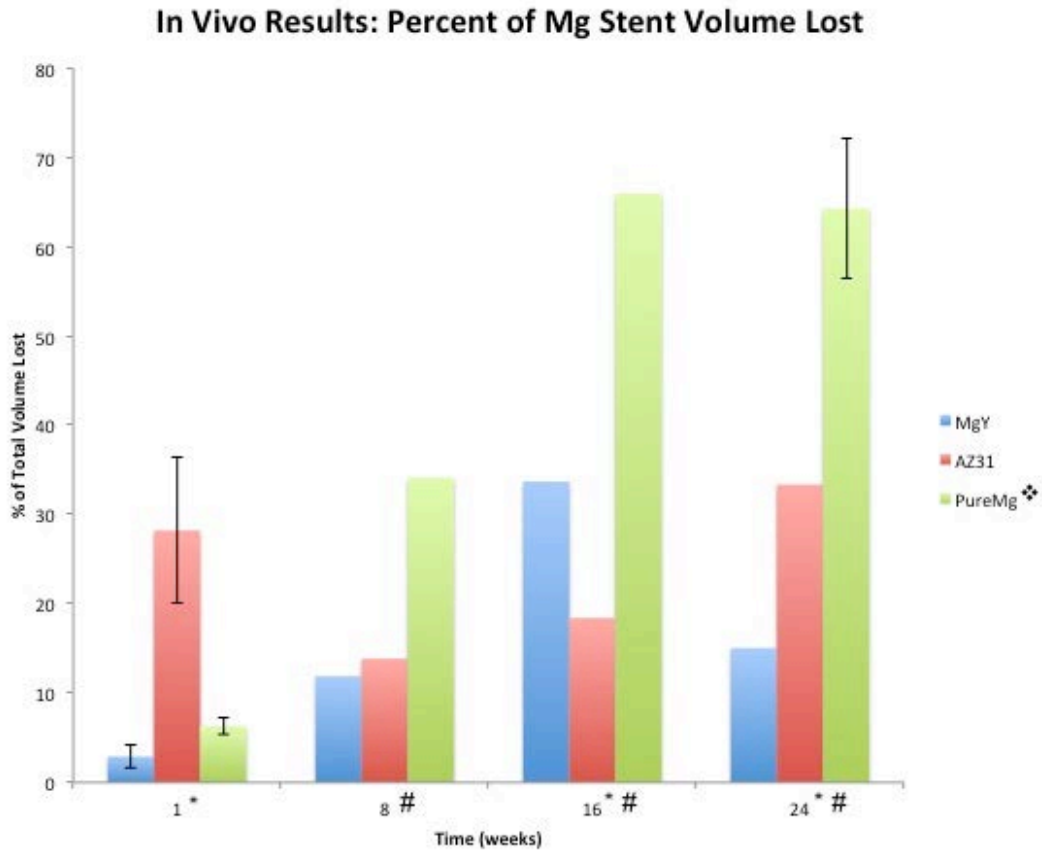
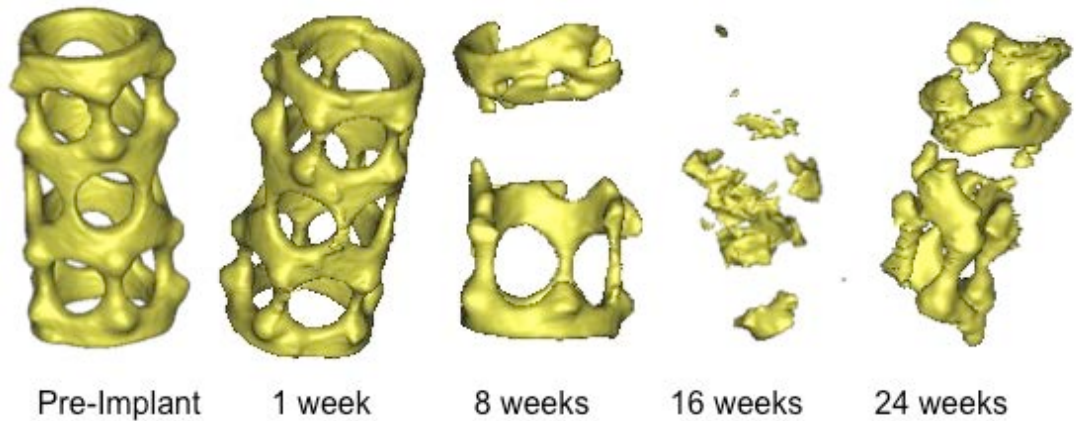


Figure 5. Percent of total volume lost during in vivo testing for each alloy at 1, 8, 16 and 24 weeks.

Significant differences among alloys and between time points are indicated by the v, \*, and #.



**Figure 6. Representative images of 3-dimensional microCT volumes for Pure Mg stents prior to implantation and at the 1, 8, 16, and 24 week time points.**

### **2.2.1.2 Histological Evaluation**

**(Figure 7 A-H)** After 1-week in vivo, H&E staining showed the presence of a normal looking epithelium without any ciliated cells noticeably present in the stented airway. There was also a prominent mononuclear cell response. Fibrous tissue appeared to surround the perimeter of the stent after 1 week, but there was no evidence of stent encapsulation. At 8-weeks, the mononuclear cell population had decreased. Although there was still some hypercellularity present after 8 weeks in vivo, the epithelium of the stented airway appeared healthy with noticeable secretory and ciliated cells. Evidence of stent encapsulation was present after 16 weeks with clear visualization of growth around what was the stent. Also, the presence of a ciliated epithelium was maintained. The encapsulated portions of the stent showed a morphology that was less organized at 24 weeks, suggesting collapse of the structure. Although a ciliated epithelium remained in particular areas, it appeared more squamous in nature. The areas of growth around the stent and throughout the graft contained evidence of vascularization as

indicated by the presence of red blood cells. Airway communication between the native airway and stented graft remained even after 24 weeks.

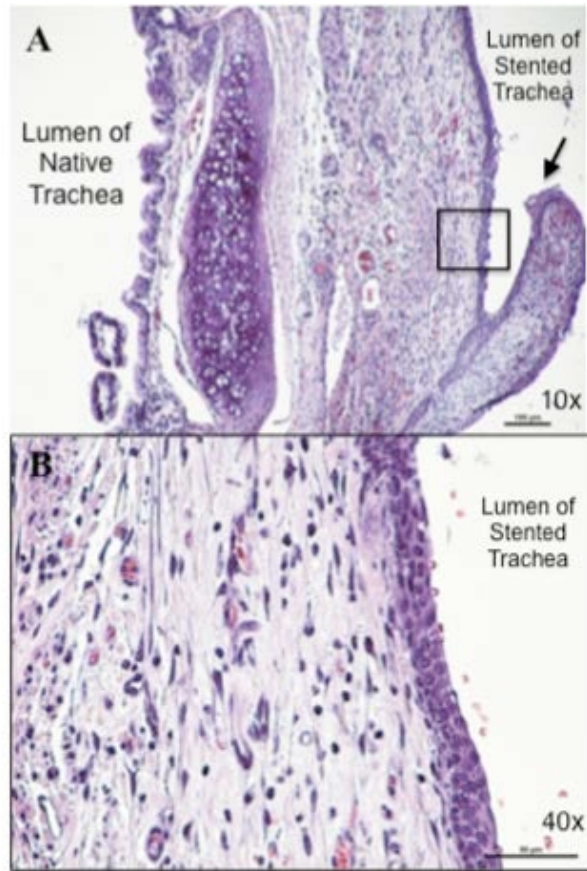


**Figure 7. A) Representative histology (H&E) from Pure Mg stents in vivo at 1 week. Cross sectional image of tracheal bypass taken to show differences in native epithelium (left) and the stented airway epithelium (right). Arrow indicates the beginning of stent incorporation. B) Boxed area of stented airway epithelium from (A) shown with higher magnification. No cilia present, but strong mononuclear presence.**

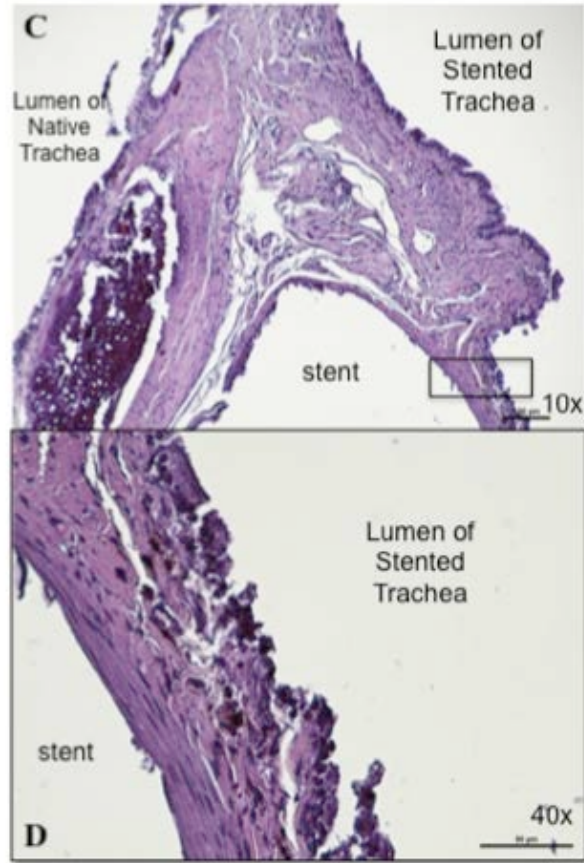


**Figure 7. C) Representative histology (H&E) from Pure Mg stents in vivo at 8 weeks showing a decreased mononuclear cell population and healthy epithelium in the stented trachea. D) Boxed area from (C) shown with higher magnification. The epithelium is disrupted but ciliated cells face the lumen of the stented trachea, while the epithelium surrounding the stent is squamous.**



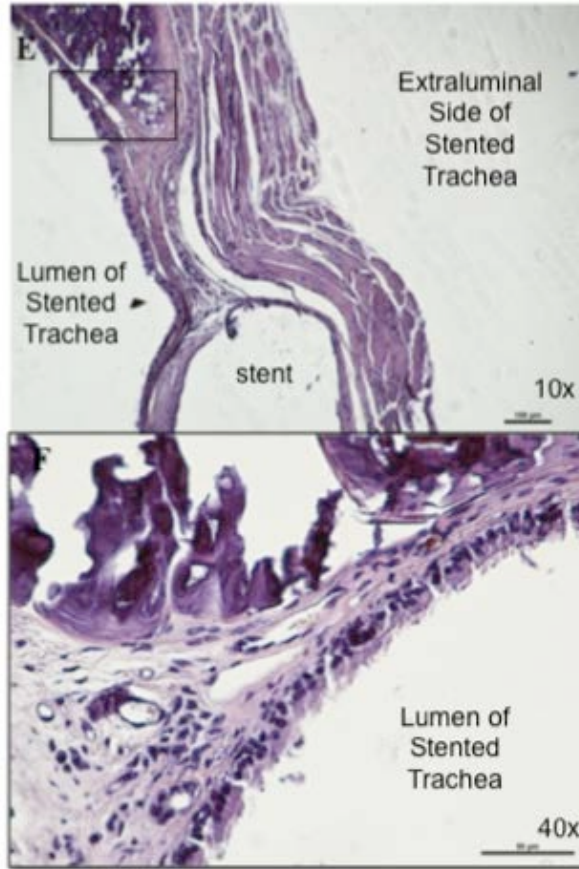


**Figure7. E) Representative histology (H&E) from Pure Mg stents in vivo at 16 weeks showing a healthy epithelium in the stented trachea. Encapsulation of the stent is also shown by the surrounding of the stent by fibrous tissue. F) Boxed area from (F) shown at higher magnification to show fully ciliated epithelial cells and secretory cells along the epithelium of the stented airway.**

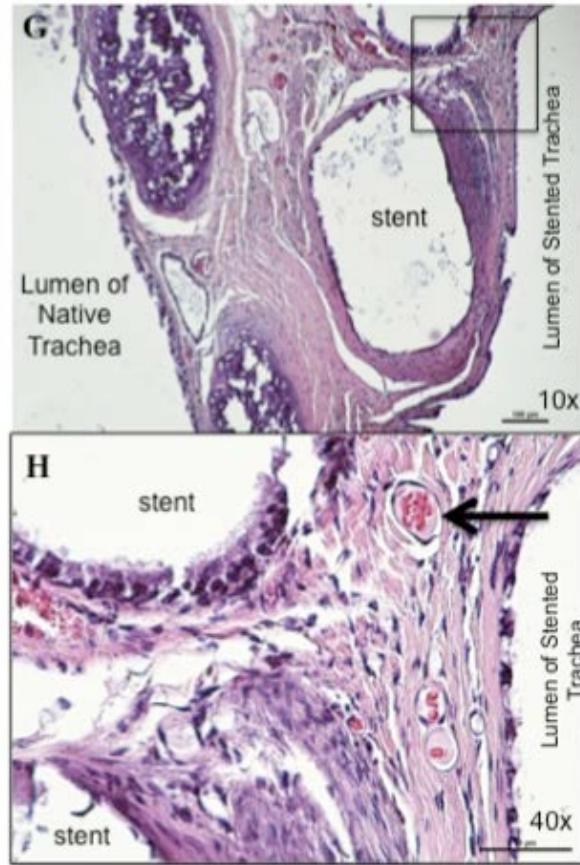


**Figure 7. G) Representative histology (H&E) from Pure Mg stents in vivo at 24 weeks. Full encapsulation of the stent is shown with a less organized morphology and areas of squamous epithelium. H) Boxed area from (H) shown with higher magnification to show presence of cilia in the areas where the Pure Mg stent was present. Arrow indicates presence of red blood cells throughout the stented trachea used for the bypass. Presence of red blood cells indicates vascularization of the graft after 24 weeks.**

## **2.2.2 AZ31**

### **2.2.2.1 Stent Volume Lost**

Corrosion of the AZ31 stent did not appear to follow any discernable trend or pattern. Total stent volume lost after 1 week was  $28.2\% \pm 16.4\%$ . Corrosion appeared to decrease after 8 weeks with

a volume loss of 13.85%  $\pm$  11.1%. After 16 weeks, total AZ31 stent volume loss increased to 18.4%  $\pm$  15.62%, and continued to a maximum stent volume loss of 33.3%  $\pm$  18.4% after 24 weeks. These findings are not consistent with the morphology of the stent as depicted by microCT imaging in **Figure 8**. No corrosion is evident after 1-week, but the structure began to change at 8 weeks. By 16 weeks, the stent structure is compromised by corrosion and fracture, which continued at the 24-week time point. The variability among AZ31 stent volume loss was so large, no patterns in corrosion were observed.

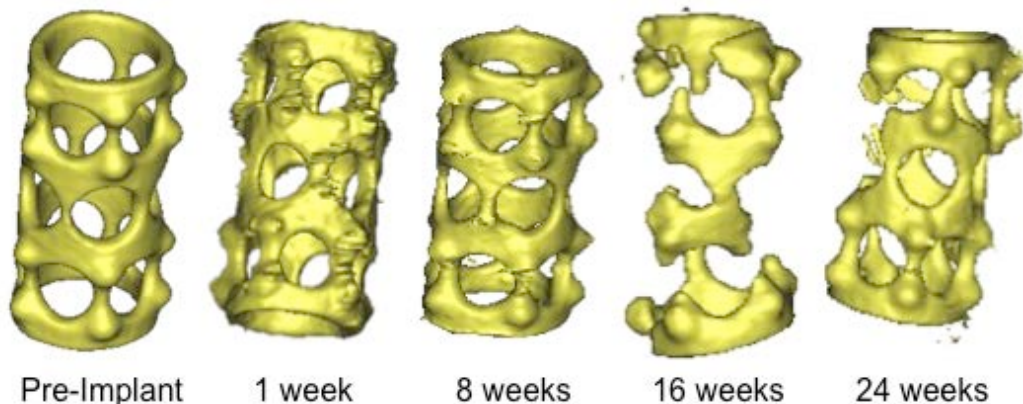


**Figure 8. Representative images of 3-dimensional microCT volumes for AZ31 stents prior to implantation and at the 1, 8, 16, and 24 week time points.**

### 2.2.2.2 Histological Evaluation

**(Figure 9A-H)** One week after AZ31 stent placement in vivo, H&E staining of the stented trachea revealed a squamous epithelium with a large presence of mononuclear cells. At the 8-week time point, histology revealed both columnar and squamous epithelium with some stent encapsulation and cell growth. The columnar epithelium had progressed to a ciliated epithelium after 16 weeks, with reduced presence of mononuclear cell response. After 24 weeks, an open lumen was maintained with the presence of ciliated cells. Overall, a columnar ciliated epithelium

with secretory cells, a mononuclear cell population with no evidence of a foreign body response, and vascularity of the graft by evidence of red blood cells was observed.

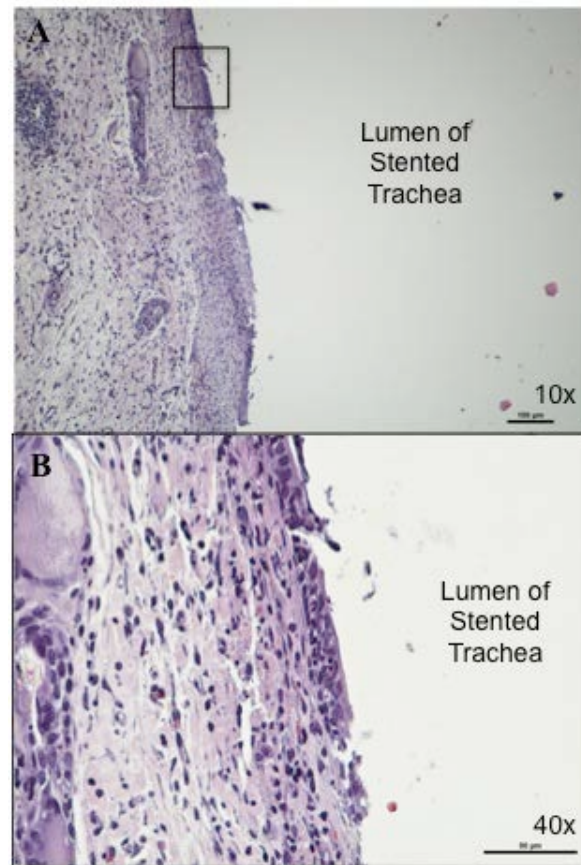


**Figure 9. A) Representative histology (H&E) from AZ31 stents in vivo at 1 week. Cross sectional image of stented trachea showing mononuclear cell population. B) Boxed area from (A) shown with higher magnification to display disruption of epithelium, most likely due to surgical placement of the stent.**

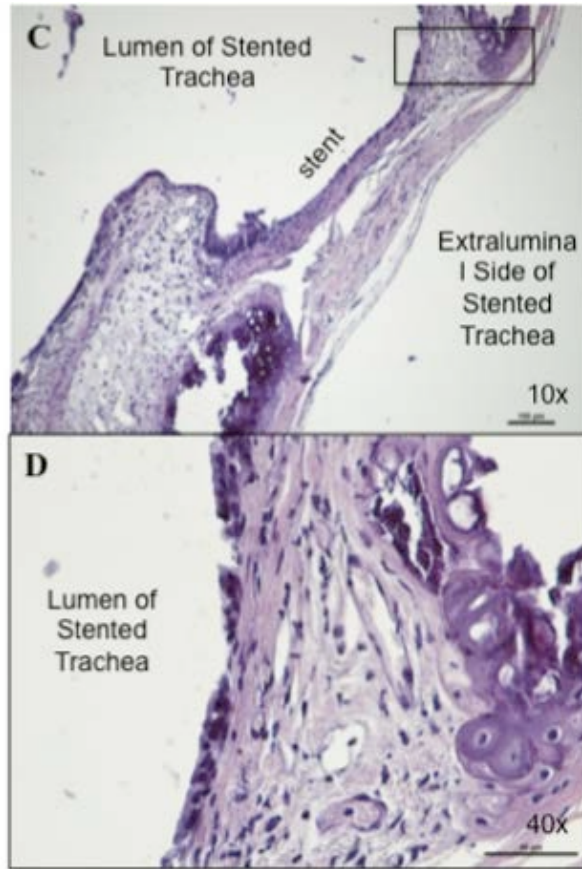


**Figure 9. C) Representative histology (H&E) from AZ31 stents in vivo at 8 weeks reveals cellular growth and areas of both columnar and squamous epithelium. Encapsulation of stent has started by 8 weeks. D) Boxed area from (C) shown at higher magnification to illustrate decreased mononuclear cell presence and no evidence of a foreign body response.**

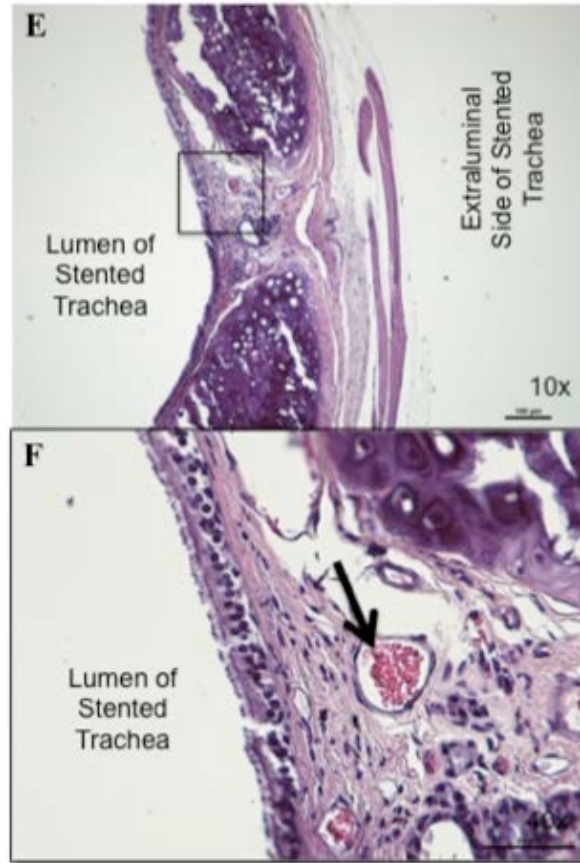


**Figure 9. E) Representative histology (H&E) from AZ31 stents in vivo at 16 weeks. F) Boxed area from (E) shown with higher magnification to demonstrate progression to a columnar, ciliated epithelium with the presence of red blood cells to indicate vascularization of the stented graft.**

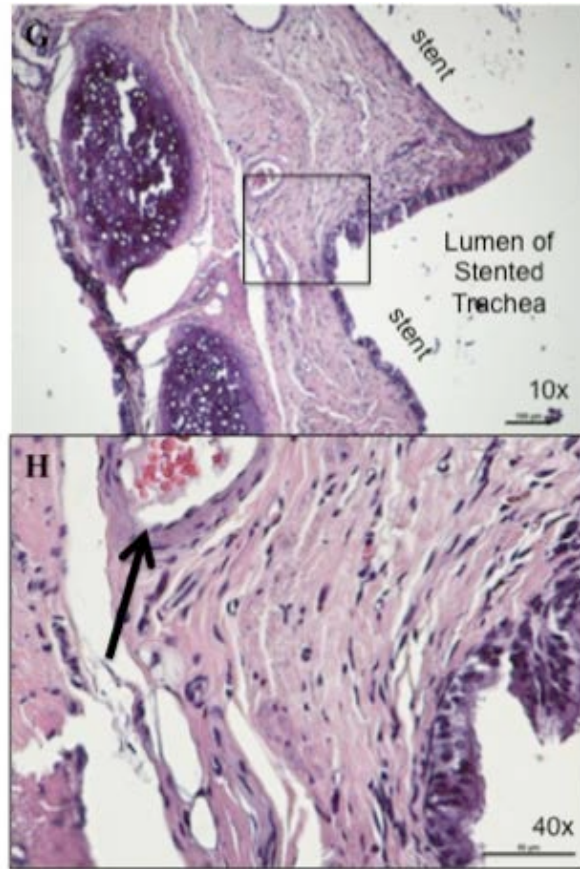


**Figure 9. G) Representative histology (H&E) from AZ31 stents in vivo at 24 weeks showing stent encapsulation and cell growth. H) Boxed area from (G) shown at higher magnification illustrating ciliated epithelium and some hypercellularity around the areas of the AZ31 stent. Arrow indicates the presence of red blood cells as evidence of vascularization of the tracheal graft after 24 weeks.**

### **2.2.3 MgY**

#### **2.2.3.1 Stent Volume Lost**

MgY stents experienced the least amount of stent volume lost among all alloys at 1 week in vivo with  $2.9\% \pm 2.5\%$ . The total stent volume lost showed a continuous increase to  $11.9\% \pm 4.4\%$

after 8 weeks and  $33.7\% \pm 21.5\%$  after 16 weeks, before decreasing to  $15.1\% \pm 13.9\%$  after 24 weeks. This corrosion behavior is similar to that of the Pure Mg stents – a continuous increase in volume loss from 1-week to a peak at 16 weeks, before slightly decreasing after 24 weeks. Although the corrosion patterns are similar to the Pure Mg stents, significant differences were observed between MgY and Pure Mg for total stent volume lost. Representative corrosion patterns of the MgY stents at each time point are illustrated in **Figure 10**. Images reveal an intact stent at 1-week, with progressive corrosion and fracture beginning at 8 weeks. By 24 weeks, the MgY stents appear completely compromised with a globular morphology.

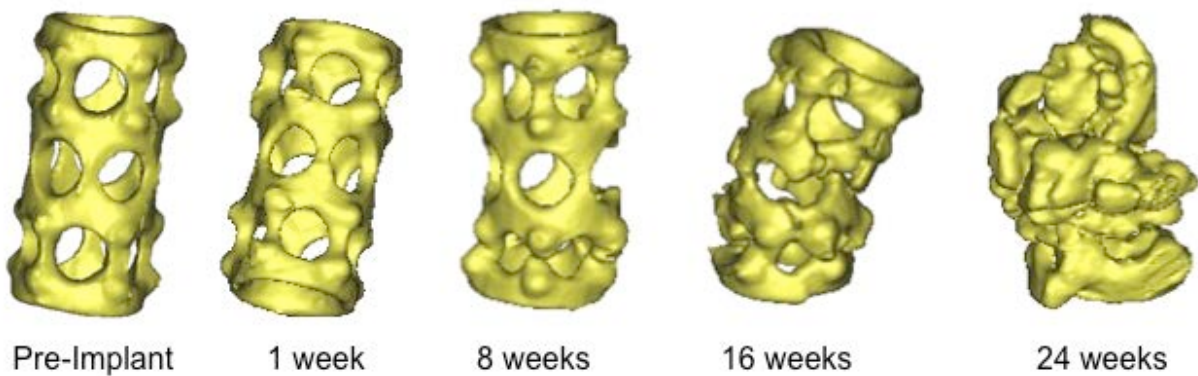


**Figure 10. Representative images of 3-dimensional microCT volumes for MgY stents prior to implantation and at the 1, 8, 16, and 24 week time points.**

### 2.2.3.2 Histological Evaluation

(**Figure 11A-H**) MgY histology revealed mononuclear cells and hypercellularity around the stented graft after 1 week in vivo. Some areas of the epithelium appeared normal, while squamous epithelium was observed in areas of contact with the stent. MgY was the only alloy to reveal a potential indication of foreign body response with a limited number of giant cells present after 1 week. By 8 weeks, an open lumen with a normal epithelium was observed with



growth and encapsulation around the stent. After 16 weeks in vivo, a prominent inflammatory response was observed in one animal that appeared to surround the graft with evidence of a foreign body response revealed by the presence of neutrophilic cells and multinucleated giant cells. A mucous plug was observed in the lumen of the graft, possibly indicating an immune response even after 24 weeks. The results suggest the possibility of an infection.

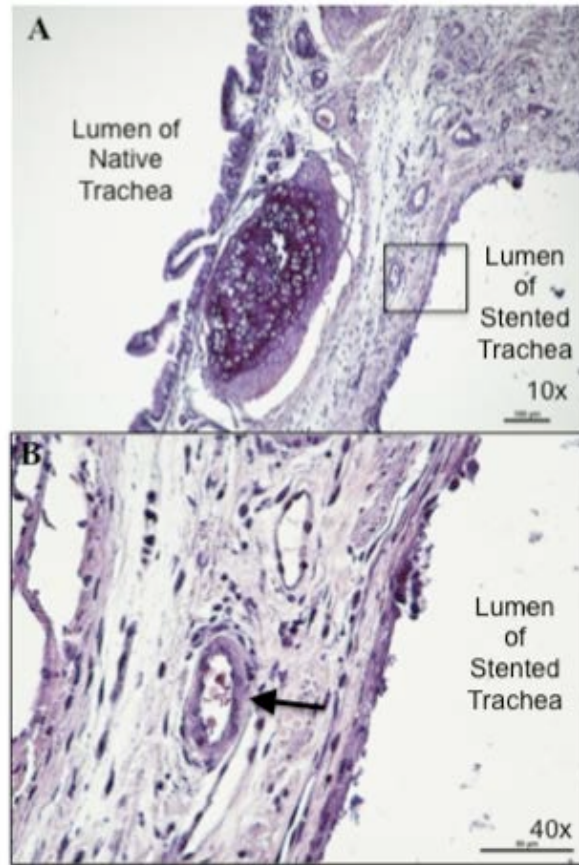


**Figure 11. A) Representative histology (H&E) from MgY stents after 1 week in vivo. Hypercellularity in the native tracheal epithelium with the presence of possible giant cells. B) Boxed area from (A) shown with higher magnification. Epithelium is disrupted and arrow indicates possible giant cell.**

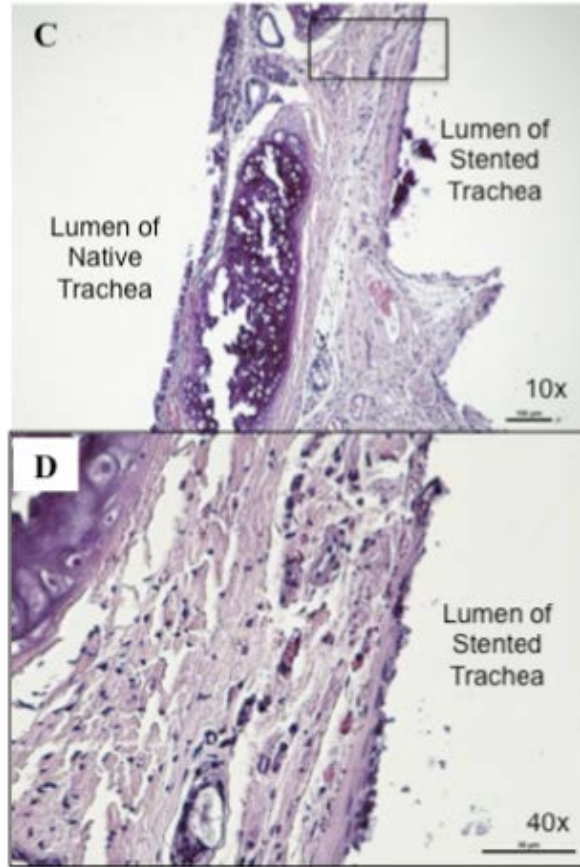


**Figure 11. C) Representative histology (H&E) from MgY stents after 8 weeks in vivo showing invaginations and encapsulation around areas of stent placement. D) Boxed area from (C) shown with higher magnification. Epithelium appeared both normal and squamous (shown).**

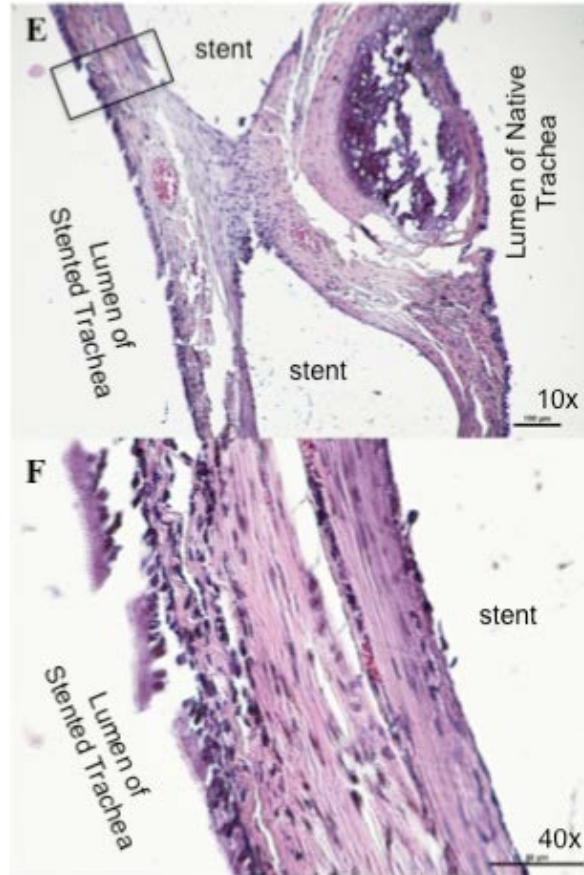


**Figure 11. E) Representative histology (H&E) from MgY stents after 16 weeks showing complete encapsulation of the stent with the presence of a ciliated epithelium. F) Boxed area from (E) shown with higher magnification. The epithelium varies depending on proximity to stent – closest to the stent, the epithelium is squamous, while the epithelium facing the lumen of the trachea is a fully ciliated epithelium with secretory cells.**

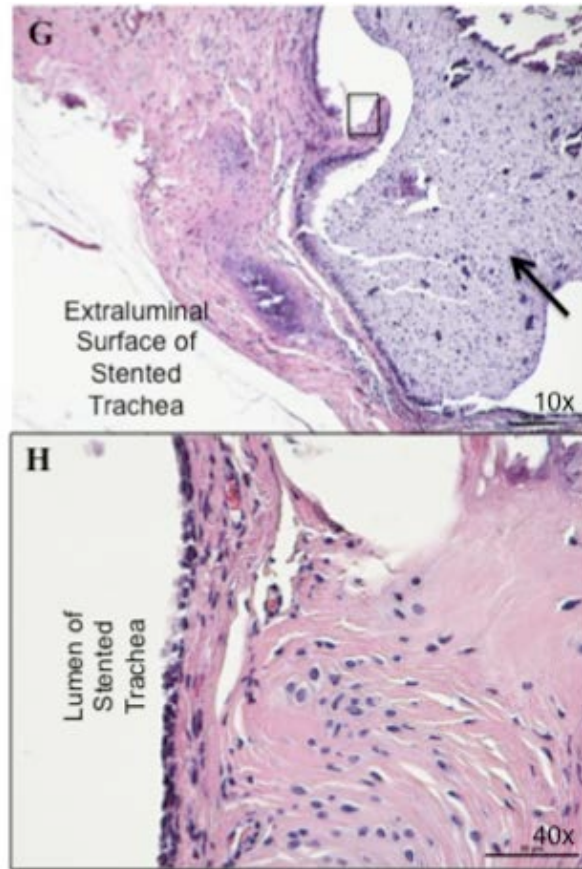


Figure 11. G) Representative histology (H&E) from MgY stents after 24 weeks showing the mucous plug found in the stented airway of n=1 animal. Arrow indicates area of mucous plug. H) Boxed area from (G) with higher magnification to show presence of a ciliated epithelium after 24 weeks. Although they are not healthy, the cilia are present even in the presence of a mucous plug.

### 2.3 SUMMARY OF IN VIVO RESULTS

Statistical analysis indicated significantly more stent corrosion for Pure Mg than for AZ31 and MgY ( $p=0.003$ ), while no significant differences were observed in stent corrosion between the magnesium alloys AZ31 and MgY ( $p=0.376$ ), as indicated in **Figure 5**. Post-hoc analysis

showed that MgY corroded the least at the 1-week time point. Pure Mg alloys showed the most corrosion with the greatest amount of total volume lost at the 16-week time point.

Corrosion results compared at early time points of 1 and 8 weeks did not have significant differences ( $p=0.633$ ), while the same is true for results compared at late time points of 16 and 24 weeks ( $p=0.999$ ). Significant differences in stent corrosion were observed between the 1-week and both the 16 and 24-week time points ( $p=0.002$ ). Comparisons of the 8-week time point with both the 16 and 24-week time points revealed significant differences in stent corrosion ( $p=0.030$  and  $p=0.034$ , respectively). Even with differences in stent corrosion at the 1-week time point, the structure of the stents remained intact. Changes in stent structure began to occur after 8 weeks for all alloys with corrosion at the thinner areas of the stent. Stent fractures lead to a compromise of the structure of the stent, usually occurring at the later time points. It is unclear whether the fractures resulted from corrosion or mechanical stresses, and results vary among alloys and time points.

In general, histology revealed similar results among all three magnesium stents. Airway communication between the stented graft and the native airway was maintained throughout the study with the tracheal bypass model. A ciliated epithelium was present after 8 weeks and persisted until 24 weeks. The MgY stents were the only stents to indicate a slight inflammatory or foreign body response, possibly due to an infection. All alloys experienced tissue growth around the stent leading to encapsulation around 16 weeks and increasing by 24 weeks. At the 24-week time point, the stented graft was vascularized by the native trachea as demonstrated by the presence of red blood cells.

### **3.0 EVALUATION OF MAGNESIUM ALLOYS IN VITRO**

#### **3.1 IN VITRO STUDY DESIGN AND METHODS**

Magnesium alloys as tracheal stents were assessed using an *in vitro* model in order to compare *in vivo* degradation results to degradation of the stent *in vitro*. The stent was placed in a decellularized lewis rat trachea and mounted in a bioreactor chamber containing extraluminal media and intraluminal media. All three alloys were evaluated in both simulated airway fluid media (Dissolution Technologies, Marques et al.) and 0.9% saline (Fisher Scientific) for a control comparison. The simulated airway fluid media contains a mixture of mucins and salts to mimic the environment of the trachea. All of the components of the SAF media are added in the following order to allow for complete dissolution: magnesium chloride (0.095 g/L), sodium chloride (6.019 g/L), potassium chloride (0.298 g/L), disodium hydrogen phosphate (0.126 g/L), sodium sulfate (0.063 g/L), calcium chloride dihydrate (0.368 g/L), sodium acetate (0.574 g/L), sodium hydrogen carbonate (2.604 g/L), sodium citrate dihydrate (0.097 g/L), and finally porcine stomach mucin (0.6 g/L). More or less mucin is added to the media in order to vary the viscosity of the SAF. A total of n=3 stents were used for each alloy and each condition. The stented decellularized trachea persisted in the bioreactor chamber for 1 week. A continuous flow pump (Ismatec) was used to circulate media at a constant rate of 0.5 mL/hour for the duration of the experiment. Polycarbonate square chambers held the stented trachea on hollow, steel rods that

allowed for internal media flow through the trachea and pump tubing. Side ports on the chambers allowed for samples to be taken from the external media of the chamber to measure the amount of magnesium present in the media. Samples of the media (0.5mL) were taken every 48 hours. In vitro degradation kinetics were assessed using inductively coupled plasma (ICP). After one week in vitro, the stents were imaged using microCT and processed for quantification of volume loss. Data from *in vivo* and *in vitro* stent degradation were compared and analyzed for statistical significance.

### **3.1.1 Assessment of Corrosion in vitro**

#### **3.1.1.1 ICP Analysis**

Inductively coupled plasma (ICP) was used to measure the amount of magnesium present in the media at 1, 3, 5, and 7 days in vitro. Standard calibrations were made to achieve baseline magnesium concentrations in parts per million (ppm). Every sample taken from the bioreactor with SAF conditions was diluted 1:20 in saline, and by diluting only SAF in saline by 1:20 a blank was also created. The blank was used to subtract the mucins and salts found in SAF and gain a more accurate measurement of magnesium at each time point. Each sample taken from the bioreactor with control conditions was also diluted 1:20 in fresh saline, and a saline blank was created.

Upon completion of ICP, the SAF and saline blanks were subtracted from the SAF and control measurements, respectively. The difference was then multiplied by 20 to achieve the amount of magnesium measured in the media at 1, 3, 5 and 7 days in vitro for both the simulated and control conditions for each magnesium stent.

### **3.1.1.2 MicroCT Analysis**

As with the *in vivo* assessment,  $\mu$ CT was used to image the tracheal stents after 1 week of *in vitro* testing. The stents were manually removed from the bioreactor chambers and gently removed from the decellularized trachea before being subjected to  $\mu$ CT imaging. The 2-D dicom files of the *in vitro* stents were processed using Mimics software. Three-dimensional volumes of the stents were generated for each of the alloys tested *in vitro* for 1 week and compared to 3-D volumes of the original stents prior to undergoing testing. The difference in volume was calculated and an overall percent of volume lost over time was quantified. Statistical analysis was performed to determine significant differences between original stent volume and stent volume at each end point for each alloy in this study.

### **3.1.1.3 Statistical Analysis**

A one-way ANOVA with Tukey's Post Hoc analysis was performed on the percent of total stent volume lost over 7 days *in vitro* for both the simulated and control conditions. Percent of total stent volume lost *in vitro* is reported as a mean  $\pm$  standard deviation.



## 3.2 RESULTS

### 3.2.1 ICP Results

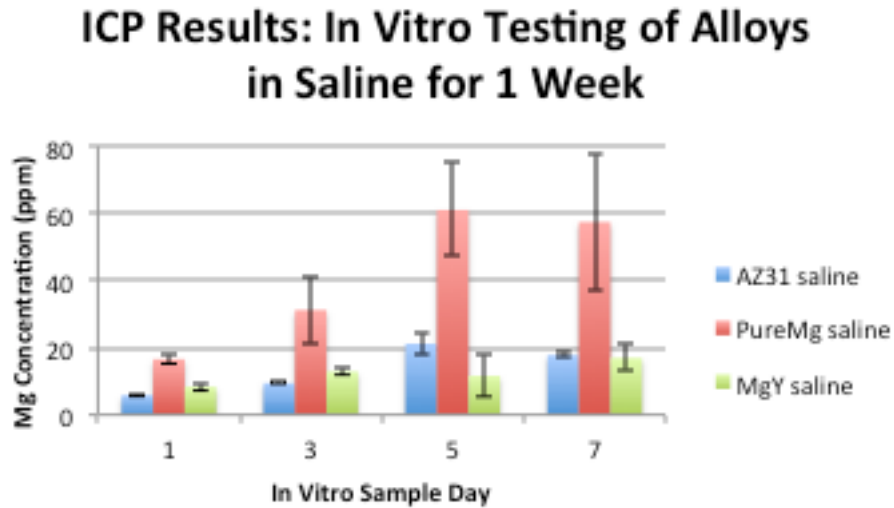


Figure 12. ICP results for each alloy showing magnesium concentration measured in SAF and in saline. Results represent averages of n=3 samples for each alloy at each time point. No significant differences were found among alloys under saline conditions, while results from Pure Mg were significantly different (❖) from AZ31 and MgY under SAF conditions.

#### 3.2.1.1 Pure Mg

Magnesium concentration measured from the Pure Mg stent in saline control media was  $16.6 \pm 2.4$  ppm at in vitro day 1. The magnesium concentration nearly doubled by day 3 ( $31.3 \pm 17.5$  ppm), peaked at day 5 ( $61.1 \pm 24.1$  ppm), and then slightly decreased by day 7 ( $57.5 \pm 35.5$  ppm). ICP measured the greatest amount of magnesium presence among all alloys from the Pure Mg in saline control media at day 5 in vitro ( $61.1 \pm 24.1$  ppm) (**Figure 13**).

Less magnesium was measured throughout SAF conditions for the Pure Mg stent compared to the saline control. An increasing trend was observed in magnesium concentration from SAF in vitro day 1 ( $9.5 \pm 2.2$  ppm) to SAF in vitro day 7. Magnesium concentration for SAF in vitro day 3 was  $10.1 \pm 2.5$  ppm. After 5 days in SAF, magnesium concentration was measured by ICP to be  $20.8 \pm 3.2$  ppm. Peak concentration of magnesium for the Pure Mg stent in SAF media was measured on day 7 with  $26.3 \pm 3.5$  ppm.

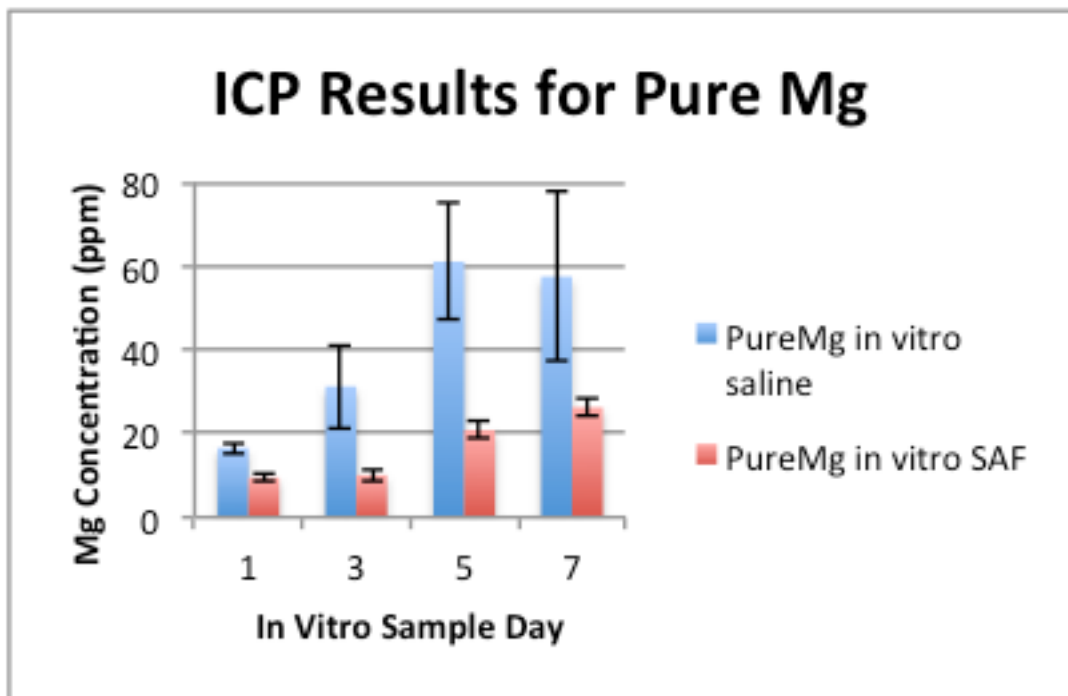


Figure 13. ICP results for Pure Mg tracheal stents, displaying average magnesium concentrations (n=3) at 1, 3, 5, and 7 days in vitro for both SAF and saline conditions.

### 3.2.1.2 AZ31

Magnesium measurements from AZ31 stents using ICP resulted in greater concentrations of magnesium under SAF conditions than under saline control conditions (**Figure 14**). At saline

control in vitro day 1, magnesium concentration was  $5.9 \pm 0.6$  ppm. In vitro day 3 AZ31 magnesium concentration steadily increased to  $9.5 \pm 0.5$  ppm, and continued to increase to a peak saline control concentration for AZ31 of  $21.2 \pm 5.7$  ppm by day 5. By day 7, magnesium concentration had decreased to  $17.8 \pm 1.4$  ppm.

Magnesium concentrations for AZ31 stents in SAF showed a steady increase from in vitro day 1 to day 7. ICP measured magnesium concentrations in SAF at  $15.4 \pm 5.7$  ppm. Day 3 magnesium concentration was measured at  $22.3 \pm 2.4$  ppm. The increasing trend continued at SAF in vitro day 5 ( $48.4 \pm 15.5$  ppm) to day 7 ( $50.9 \pm 7.7$  ppm).

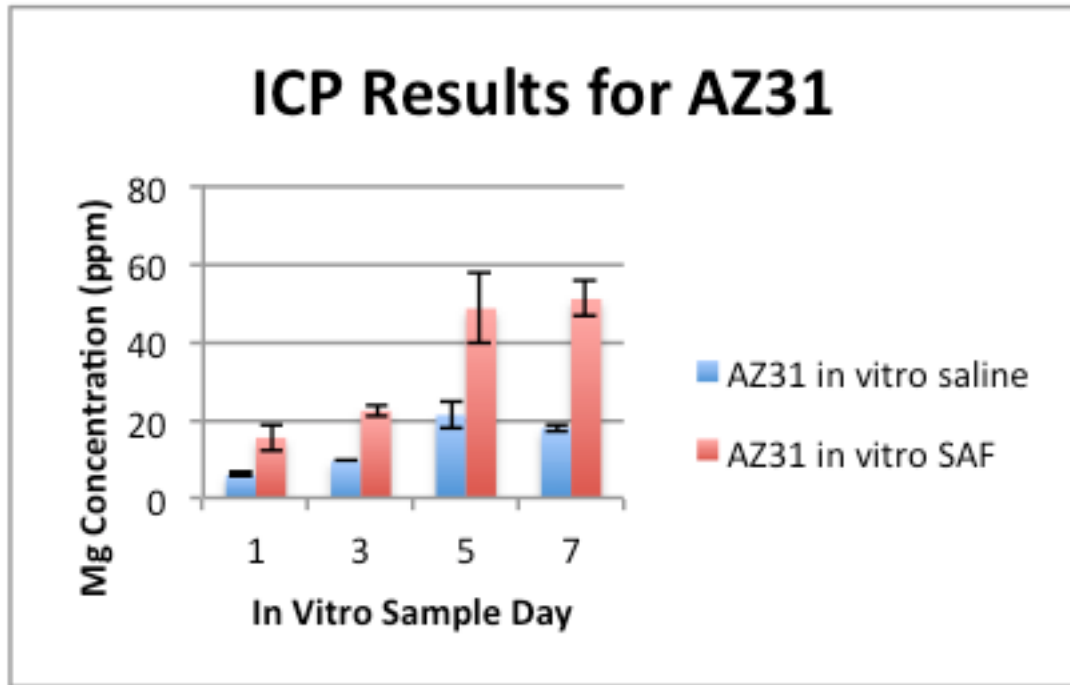


Figure 14. ICP results for AZ31 tracheal stents, displaying average magnesium concentrations (n=3) at 1, 3, 5, and 7 days in vitro for both SAF and saline conditions.

### 3.2.1.3 MgY

For the MgY stents in the saline control conditions, magnesium concentrations steadily trended upward from in vitro day 1 to in vitro day 7 (**Figure 15**). ICP measured a magnesium concentration for MgY saline day 1 at  $8.4 \pm 1.9$  ppm, and increased to  $12.9 \pm 1.7$  ppm at day 3.

By in vitro day 5, the magnesium concentration for the saline control conditions for MgY slightly decreased to  $11.6 \pm 10.7$  ppm, before increasing to  $16.9 \pm 6.9$  ppm by day 7.

Greater magnesium concentration was measured from the SAF conditions for MgY stents in vitro. No steady, increasing trend for the SAF conditions for MgY stents was observed. ICP

measurements resulted in similar day 1 and day 3 magnesium concentration results ( $7.1 \pm 4.3$  ppm and  $7.3 \pm 4.7$  ppm), and increased but similar measurements at day 5 and day 7 ( $30.6 \pm 10.6$  ppm and  $33.5 \pm 9.7$  ppm).

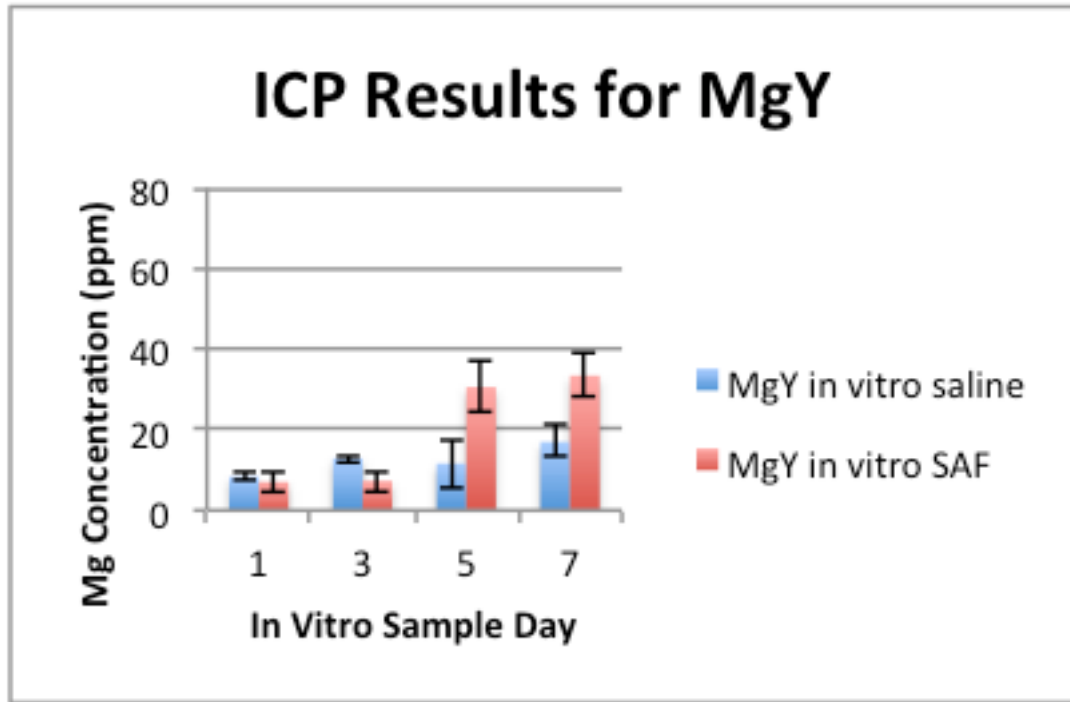


**Figure 15.** ICP results for MgY tracheal stents, displaying average magnesium concentrations (n=3) at 1, 3, 5, and 7 days in vitro for both SAF and saline conditions.

### 3.2.2 MicroCT Analyses

After the stents were tested for 1 week in vitro under both SAF and control conditions, microCT images were obtained and the volume loss was calculated. The in vitro stent volumes were compared to the in vivo stent volumes at the 1-week time point.

### 3.2.2.1 Pure Mg

Percent of total volume lost for a Pure Mg stent after 1 week in vitro under SAF conditions was  $4.55\% \pm 8.67\%$ . Saline control conditions for 1 week in vitro resulted in  $21.81\% \pm 16.98\%$  total stent volume lost. The results from SAF conditions are more closely related to the results from total Pure Mg stent volume lost after 1 week in vivo, 2.34% total volume lost (**Figure 16 and Figure 17**).

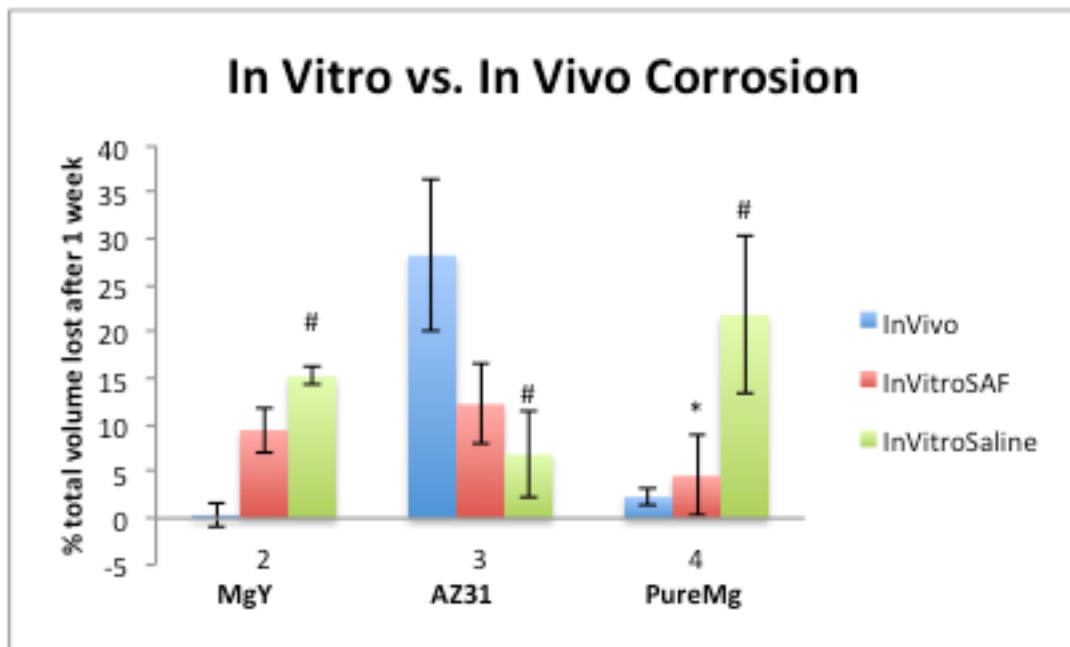


**Figure 16.** Bar graph summarizing the comparison of corrosion after 1 week in vivo to 1 week in vitro under both SAF and saline conditions. The (#) indicates significant differences were observed between all alloys under the saline in vitro control conditions, while the (\*) indicates only Pure Mg experienced significantly different results under SAF in vitro conditions.







	SAF	Saline
Pure Mg		
AZ31		
MgY		

Figure 17. Representative 3-dimensional microCT images of Pure Mg, AZ31, and MgY stents after 1 week of in vitro testing in SAF media and saline control conditions.

### 3.2.2.2 AZ31

Greater total stent volume lost was observed after 1 week under SAF in vitro conditions with  $12.24\% \pm 8.43\%$  total stent volume lost. This result is approximately double the results of  $6.82\%$

$\pm 9.12\%$  total stent volume lost after 1 week in vitro under control conditions. Percent of total stent volume lost after 1 week in vivo appears much greater than the in vitro results with  $28.19\% \pm 7.71\%$  total stent volume lost, (**Figure 16 and Figure 17**).

### 3.2.2.3 MgY

While MgY stents experienced very little ( $0.35\% \pm 2.53\%$ ) total volume loss after 1 week in vivo, the results from 1 week in vitro demonstrated greater volume loss under saline control conditions with  $15.22\% \pm 1.99\%$  total volume lost. The MgY stents under SAF conditions for 1 week in vitro experienced  $9.46\% \pm 4.95\%$  total stent volume lost, (**Figure 16 and Figure 17**).

### 3.2.3 Statistical Analysis

Significant differences in ICP results were observed between the magnesium stents under SAF conditions ( $p=0.019$ ), while no significant differences between magnesium stents were observed for the saline control conditions ( $p=0.224$ ), (**Figure 16**). Magnesium content measured from AZ31 and MgY stents were not significantly different under SAF conditions, however the magnesium content measured for Pure Mg under SAF conditions was significantly different from AZ31 ( $p=0.035$ ) and MgY ( $p=0.029$ ). No significant differences in magnesium concentration were observed between any of the magnesium stents under saline control conditions.



When comparing the 1, 3, 5 and 7 day time points under SAF conditions, no significant differences between magnesium stents were observed ( $p=0.478$ ). Under saline control conditions, however, significant differences were observed between magnesium stents over time ( $p=0.031$ ), but no significant differences were found among ICP results at 1, 3, 5, and 7 days.

### **3.3 SUMMARY OF IN VITRO RESULTS**

ICP allowed for the measurement of magnesium concentration in media at 48 hour time points throughout 1 week. The measurement of magnesium in the media is representative of the amount of magnesium lost from the stent. Measurements from ICP revealed the most magnesium was lost on day 5 of the Pure Mg in saline control media. Pure Mg stents also experienced the greatest volume lost among the 3 stents under saline control conditions after 1 week in vitro. The AZ31 alloy experienced the most magnesium loss on in vitro day 7 under SAF conditions. This is also consistent with the greatest amount of stent volume lost according to microCT analysis among the alloys under SAF conditions after 1 week in vitro.

All 3 of the magnesium stents experienced greater correlation between volume loss after 1 week in vivo and volume loss after 1 week in vitro under SAF conditions. Statistical analysis suggests no differences among magnesium stents under saline control conditions, while significant differences are found under simulated conditions. These results suggest the simulated conditions are more accurately predicting the behavior of magnesium stents after 1 week in vivo.

## 4.0 DISCUSSION

Both in vitro and in vivo testing of magnesium alloys as tracheal stents are necessary to predict and understand the degradation process of the metal. The results of this study show preliminary evidence supporting further investigation for use of magnesium alloys as a potential material for a degradable tracheal stent.

Mild evidence of a foreign body response to the MgY stents was observed in vivo with the isolated presence of a possible foreign body giant cell after 1 week and hypercellularity with neutrophils and multinucleated giant cells after 16 and 24 weeks, although the later result may have been caused by infection. Both AZ31 and Pure Mg stents did not display any signs of an inflammatory or host response throughout the in vivo study. Histological analysis of all stents revealed the presence of a normal, ciliated epithelium in the stented airway by 8 weeks and persisting after 24 weeks. Although present, the epithelium of the stented airway appeared more squamous in nature by the 24 week time point. After 1 week in vivo, the stented airway also appeared squamous in some areas, but this may have been the result of surgical manipulation since it takes time for the graft to become revascularized after transplantation. By 8 weeks, a ciliated epithelium was observed for all stents. Encapsulation of the stents began between the 8 and 16-week time points.

Little is known about the effects of magnesium on the airway, and evidence of a normal and functional airway epithelium following magnesium stent placement are encouraging results.

Because this study was limited by magnesium stents with a geometry that was not optimized, the tracheal bypass model was used for tracheal stent evaluation. It is unknown whether similar results could be achieved without the bypass model and optimized stent geometry. It would also be interesting to compare an in vivo study using a tracheal bypass model, but place the stent in the native trachea and allow for the donor trachea to truly bypass the stented native airway. Because of limitations in achieving a machinable and appropriately sized rat tracheal stent, we did not try this alternative surgical model.

In using the tracheal bypass model for the evaluation of the magnesium stents, we did not include a control group. The control group would have had the tracheal bypass but without a stent present in the donor tracheal graft. The lack of the control group leads to the question of what would be seen in the progression of the airway epithelium. Presumably the initial disruption of the airway epithelium would not occur because there would be no stent placement. Having a control group for comparison would allow for understanding into how the magnesium truly affected the health, morphology, and persistence of the airway epithelium.

MicroCT imaging provided insight into the corrosion patterns of the magnesium stents over time. By 16 or even 8 weeks, the stents appeared compromised with total stent volume losses between 18 and 66% after 16 weeks. As expected, the Pure Mg stent did experience greater corrosion in vivo than the magnesium alloys. MgY and AZ31 both experienced a maximum of 33% total stent volume lost, while MgY peaked after 16 weeks and AZ31 did not reach maximum volume loss until 24 weeks. Visually, the compromised structure of the MgY stents can be qualitatively observed as more compromised than that of the AZ31 stent, even though the stents experienced similar amounts of total volume lost. This could be the result of the alloy composition, or even the tensions experienced in vivo.

The hypothesis from specific aim 1 was successful in predicting less degradation for the AZ31 and MgY alloys compared to the Pure Mg stents. Statistical analysis also supported the hypothesis that differences in volume lost were observed between the early and late time points, suggesting a pattern for rate of degradation.

Results from ICP also partially supported the hypothesis from specific aim 2, as Pure Mg experienced the greatest volume lost in vivo and also registered the highest amount of magnesium measured in vitro. MicroCT results also revealed the closest correlation between magnesium stent volume lost at 1 week in vivo and after 1 week in vitro under SAF conditions. Differences between the in vitro results of saline control conditions and the in vivo results from 1 week, as compared to the SAF in vitro results, suggest the SAF media is contributing to creating an environment in vitro that is more closely related to an in vivo airway environment. Because the bioreactors used to evaluate the magnesium stents in vitro were continuous flow, the varying pressures associated with respiration were not applied to the stents in vitro. The tracheal bypass model also places the stented airway in a partially passive trachea environment. As a result, the continuous flow system may be a good model for comparing in vitro results to the in vivo bypass model. Similarities between in vitro and in vivo results are very encouraging for the evaluation of magnesium alloys. Historically, in vitro evaluation of magnesium could not be depended on to accurately predicted in vivo behavior. To further address the limitations of the in vitro study, magnesium alloys should be evaluated at later time points in vitro and compared to later time points in vivo.

An important limitation of the in vivo study was that the trachea stent intended for treatment of tracheal stenosis was applied to a normal, healthy trachea in a bypass model. Because the stent geometry was not yet optimized and little is known about the use of

magnesium in the trachea, this study aimed to evaluate the effects of magnesium on the airway environment. Histological analysis demonstrated minimal effects of magnesium on the function of the airway environment at early time points (1 week) and up to 24 weeks. Another study evaluating the effects of magnesium on the trachea at later time points of 6 months to 1 year, could provide further understanding on the longer term effects of magnesium on the airway environment.

## 5.0 CONCLUSIONS

Tracheal stents successfully manage adult airway obstructions, including tracheal stenosis, but are used as a treatment option of last resort for pediatric patients because of their permanent nature. A degradable tracheal stent would provide pediatric patients the opportunity for growth potential while maintaining an open lumen. The magnesium alloys evaluated in this study demonstrate potential for use in the tracheal environment. More studies will be necessary to further develop the stent design and optimize mechanical properties in order to support a pediatric airway with tracheal stenosis. This study illustrated the trachea's tolerance and acceptance of magnesium after 6 months with minimal foreign body response and without any negative effects on airway function. Initial in vitro studies using SAF provide support for additional in vitro testing to more closely mimic the response of magnesium in vivo.

## BIBLIOGRAPHY

1. Jungebluth, P., Moll, G., Baiguera, S. & Macchiarini, P. Tissue-engineered airway: a regenerative solution. *Clin. Pharmacol. Ther.* **91**, 81–93 (2012).
2. Bardin, P. G., Johnston, S. L. & Hamilton, G. Middle airway obstruction--it may be happening under our noses. *Thorax* **68**, 396–398 (2013).
3. Yong, M. S. *et al.* Surgical management of pulmonary artery sling in children. *J. Thorac. Cardiovasc. Surg.* **145**, 1033–1039 (2013).
4. Tatekawa, Y. & Muraji, T. Surgical strategy for acquired tracheomalacia due to innominate artery compression of the trachea. *Eur J Cardiothorac Surg* **39**, 412–413 (2011).
5. Maksoud-Filho, J. G., Gonçalves, M. E. P., Cardoso, S. R. & Tannuri, U. Early diagnostic and endoscopic dilatation for the treatment of acquired upper airway stenosis after intubation in children. *J. Pediatr. Surg.* **43**, 1254–1258 (2008).
6. Gallagher, T. Q. & Hartnick, C. J. Tracheal resection and reanastomosis. *Adv. Otorhinolaryngol.* **73**, 50–57 (2012).
7. Zaima, A. *et al.* Long-term T-tube stenting as definitive treatment of severe acquired subglottic stenosis in children. *J. Pediatr. Surg.* **45**, 996–999 (2010).
8. Xu, X. *et al.* Treatment of congenital tracheal stenosis by balloon-expandable metallic stents in paediatric intensive care unit. *Interact Cardiovasc Thorac Surg* **14**, 548–550 (2012).

9. Ng, A. H. C., Ng, N. S. P., Zhu, G. H., Lim, L. H. Y. & Venkatraman, S. S. A fully degradable tracheal stent: in vitro and in vivo characterization of material degradation. *J. Biomed. Mater. Res. Part B Appl. Biomater.* **100**, 693–699 (2012).
10. Antón-Pacheco, J. L. *et al.* The role of airway stenting in pediatric tracheobronchial obstruction. *Eur J Cardiothorac Surg* **33**, 1069–1075 (2008).
11. Preciado, D. & Zalzal, G. Laryngeal and tracheal stents in children. *Curr Opin Otolaryngol Head Neck Surg* **16**, 83–85 (2008).
12. Brigger, M. T. & Boseley, M. E. Management of tracheal stenosis. *Curr Opin Otolaryngol Head Neck Surg* (2012).doi:10.1097/MOO.0b013e328358566d
13. Mainwaring, R. D. *et al.* Surgical reconstruction of tracheal stenosis in conjunction with congenital heart defects. *Ann. Thorac. Surg.* **93**, 1266–72– discussion 1272–3 (2012).
14. Charokopos, N. *et al.* The management of post-intubation tracheal stenoses with self-expandable stents: early and long-term results in 11 cases. *Eur J Cardiothorac Surg* **40**, 919–924 (2011).
15. Nicolai, T. Airway stents in children. *Pediatr. Pulmonol.* **43**, 330–344 (2008).
16. Noppen, M., Stratakos, G., D'Haese, J., Meysman, M. & Vincken, W. Removal of covered self-expandable metallic airway stents in benign disorders: indications, technique, and outcomes. *Chest* **127**, 482–487 (2005).
17. Moravej, M. & Mantovani, D. Biodegradable metals for cardiovascular stent application: interests and new opportunities. *Int J Mol Sci* **12**, 4250–4270 (2011).
18. Serruys, P. W., de Jaegere, P. & Kiemeneij, F. A comparison of balloon-expandable-stent implantation with balloon angioplasty in patients with coronary artery disease. ... *England Journal of ...* (1994).
19. Rassaf, T., Steiner, S. & Kelm, M. Postoperative care and follow-up after coronary stenting. *Dtsch Arztebl Int* **110**, 72–82 (2013).



20. Mitsuoka, M., Sakuragi, T. & Itoh, T. Clinical benefits and complications of Dumon stent insertion for the treatment of severe central airway stenosis or airway fistula. *Gen Thorac Cardiovasc Surg* **55**, 275–280 (2007).
21. Lawton, B. & Gungor, A. Airway salvation after failed anterior graft in a child with long segment stenosis. *Am J Otolaryngol* (2013).doi:10.1016/j.amjoto.2013.02.009
22. Mroz, R. M. *et al.* Severe respiratory distress caused by central airway obstruction treated with self-expandable metallic stents. *J. Physiol. Pharmacol.* **59 Suppl 6**, 491–497 (2008).
23. Coordes, A., Todt, I., Ernst, A. & Seidl, R. O. Multi-stage surgery for airway patency after metallic stent removal in benign laryngotracheal airway disease in two adolescents. *Int. J. Pediatr. Otorhinolaryngol.* (2013).doi:10.1016/j.ijporl.2013.02.012
24. Murthy, S. C., Gildea, T. R. & Mehta, A. C. Removal of self-expandable metallic stents: is it possible? *Semin Respir Crit Care Med* **25**, 381–385 (2004).
25. Vondrys, D., Elliott, M. J., McLaren, C. A., Noctor, C. & Roebuck, D. J. First experience with biodegradable airway stents in children. *Ann. Thorac. Surg.* **92**, 1870–1874 (2011).
26. Peuster, M. *et al.* A novel approach to temporary stenting: degradable cardiovascular stents produced from corrodible metal-results 6-18 months after implantation into New Zealand white rabbits. *Heart* **86**, 563–569 (2001).
27. Heublein, B. *et al.* Biocorrosion of magnesium alloys: a new principle in cardiovascular implant technology? *Heart* **89**, 651–656 (2003).
28. Chen, D. *et al.* Biocompatibility of magnesium-zinc alloy in biodegradable orthopedic implants. *Int. J. Mol. Med.* **28**, 343–348 (2011).
29. Witte, F. The history of biodegradable magnesium implants: a review. *Acta Biomater* **6**, 1680–1692 (2010).
30. Zartner, P., Cesnjevar, R., Singer, H. & Weyand, M. First successful implantation of a biodegradable metal stent into the left pulmonary artery of a preterm baby. *Catheter Cardiovasc Interv* **66**, 590–594 (2005).

31. Schranz, D., Zartner, P., Michel-Behnke, I. & Akintürk, H. Bioabsorbable metal stents for percutaneous treatment of critical recoarctation of the aorta in a newborn. *Catheter Cardiovasc Interv* **67**, 671–673 (2006).
32. Erbel, R. *et al.* Temporary scaffolding of coronary arteries with bioabsorbable magnesium stents: a prospective, non-randomised multicentre trial. *Lancet* **369**, 1869–1875 (2007).
33. Gourgoulianis, K. I., Chatziparasidis, G., Chatziefthimiou, A. & Molyvdas, P. A. Magnesium as a relaxing factor of airway smooth muscles. *J Aerosol Med* **14**, 301–307 (2001).
34. Pollart, S. M., Compton, R. M. & Elward, K. S. Management of acute asthma exacerbations. *Am Fam Physician* **84**, 40–47 (2011).
35. SEELIG, M. G. A STUDY OF MAGNESIUM WIRE AS AN ABSORBABLE SUTURE AND LIGATURE MATERIAL. *Arch Surg* **8**, 669–680 (1924).
36. Witte, F. *et al.* In vitro and in vivo corrosion measurements of magnesium alloys. *Biomaterials* **27**, 1013–1018 (2006).
37. Hänzi, A. C., Gerber, I., Schinhammer, M., Löffler, J. F. & Uggowitzer, P. J. On the in vitro and in vivo degradation performance and biological response of new biodegradable Mg-Y-Zn alloys. *Acta Biomater* **6**, 1824–1833 (2010).
38. Di Mario, C. *et al.* Drug-eluting bioabsorbable magnesium stent. *J Interv Cardiol* **17**, 391–395 (2004).
39. Kannan, M. B. & Raman, R. K. S. In vitro degradation and mechanical integrity of calcium-containing magnesium alloys in modified-simulated body fluid. *Biomaterials* **29**, 2306–2314 (2008).
40. Scheideler, L. *et al.* Comparison of different in vitro tests for biocompatibility screening of Mg alloys. *Acta Biomater* (2013).doi:10.1016/j.actbio.2013.02.020
41. United States Food and Drug Administration, FDA.